URL: https://atvb-submit.aha-journals.org

Manuscript Number: ATVB/2017/310388R2

Title: Inhibition of endothelial NOTCH1 signaling attenuates inflammation by reducing cytokine-mediated histone acetylation at inflammatory enhancers

Authors: Lars la Cour Poulsen (Oslo University Hospital), Reidunn Edelmann (Haukeland University Hospital and University of Bergen), Stig Krüger (Oslo University Hospital and University of Oslo), Rodrigo Diéguez-Hurtado (Max Planck Institute for Molecular Biomedicine), Akshay Shah (University of Oslo), Tor Espen Stav-Noraas (Oslo University Hospital and University of Oslo), Anastasia Renzi (Oslo University Hospital Rikshospitalet and University of Oslo), Monika Szymanska (Oslo University Hospital), Junbai Wang (Oslo University Hospital), Manuel Ehling (University of Münster), Rui Benedito (Centro Nacional Investigaciones Cardiovasculares), Monika Kasprzycka (Oslo University Hospital), Espen Bækkevold (Oslo University and University of Oslo), Olav Sundnes (Oslo University Hospital and University of Oslo), Kim Midwood (University of Oxford), Helge Scott (Oslo University Hospital and Oslo University), Philippe Collas (University of Oslo), Christian Siebel (Genentech), Ralf Adams (Max Planck Institute for Molecular Biomedicine), Guttorm Haraldsen (Oslo University Hospital), Eirik Sundlisæter (Oslo University Hospital and University of Oslo), and Johanna Hol (Department of Pathology, Oslo University Hospital Ullevål, University of Oslo)

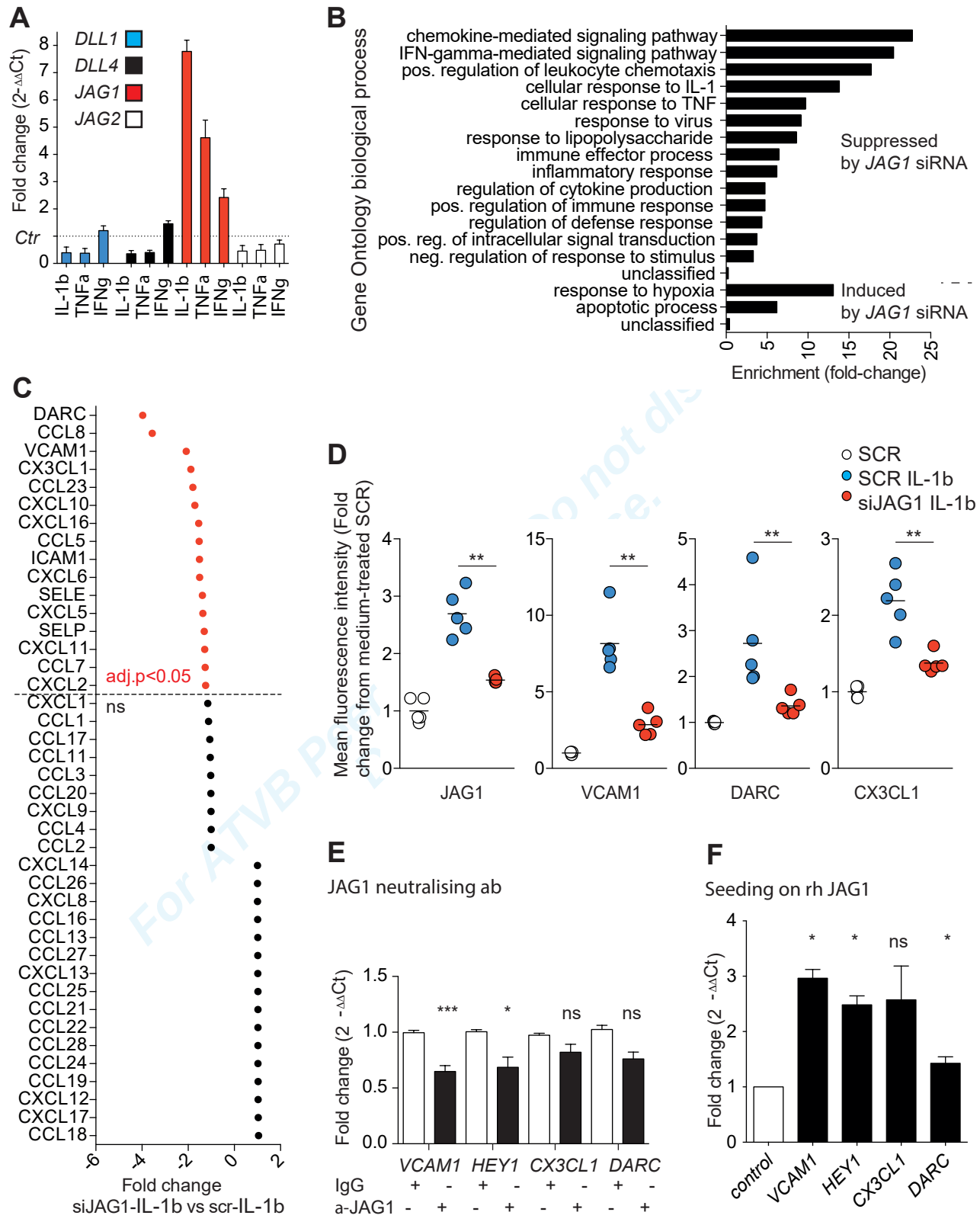
A
DLL1
DLL4
JAG1
JAG2
Fold change (2-ΔΔCt)
Ctr
IL-1b
TNFa
IFNg
B
Gene Ontology biological process
chemokine-mediated signaling pathway
IFN-gamma-mediated signaling pathway
pos. regulation of leukocyte chemotaxis
cellular response to IL-1
cellular response to TNF
response to virus
response to lipopolysaccharide
immune effector process
inflammatory response
regulation of cytokine production
pos. regulation of immune response
regulation of defense response
pos. reg. of intracellular signal transduction
neg. regulation of response to stimulus
unclassified
response to hypoxia
apoptotic process
unclassified
Suppressed by JAG1 siRNA
Induced by JAG1 siRNA
Enrichment (fold-change)
C
DARC
CCL8
VCAM1
CX3CL1
CCL23
CXCL10
CXCL16
CCL5
ICAM1
CXCL6
SELE
CXCL5
SELP
CXCL11
CCL7
CXCL2
adj.p<0.05
CXCL1
ns
CCL1
CCL17
CCL11
CCL3
CCL20
CXCL9
CCL4
CCL2
CXCL14
CCL26
CXCL8
CCL16
CCL13
CCL27
CXCL13
CCL25
CCL21
CCL22
CCL28
CCL24
CCL19
CXCL12
CXCL17
CCL18
Fold change
siJAG1-IL-1b vs scr-IL-1b
D
SCR
SCR IL-1b
siJAG1 IL-1b
Mean fluorescence intensity (Fold change from medium-treated SCR)
JAG1
VCAM1
DARC
CX3CL1
E
JAG1 neutralising ab
Fold change (2 -ΔΔCt)
VCAM1
HEY1
CX3CL1
DARC
IgG
a-JAG1
F
Seeding on rh JAG1
Fold change (2 -ΔΔCt)
control
VCAM1
HEY1
CX3CL1
DARC

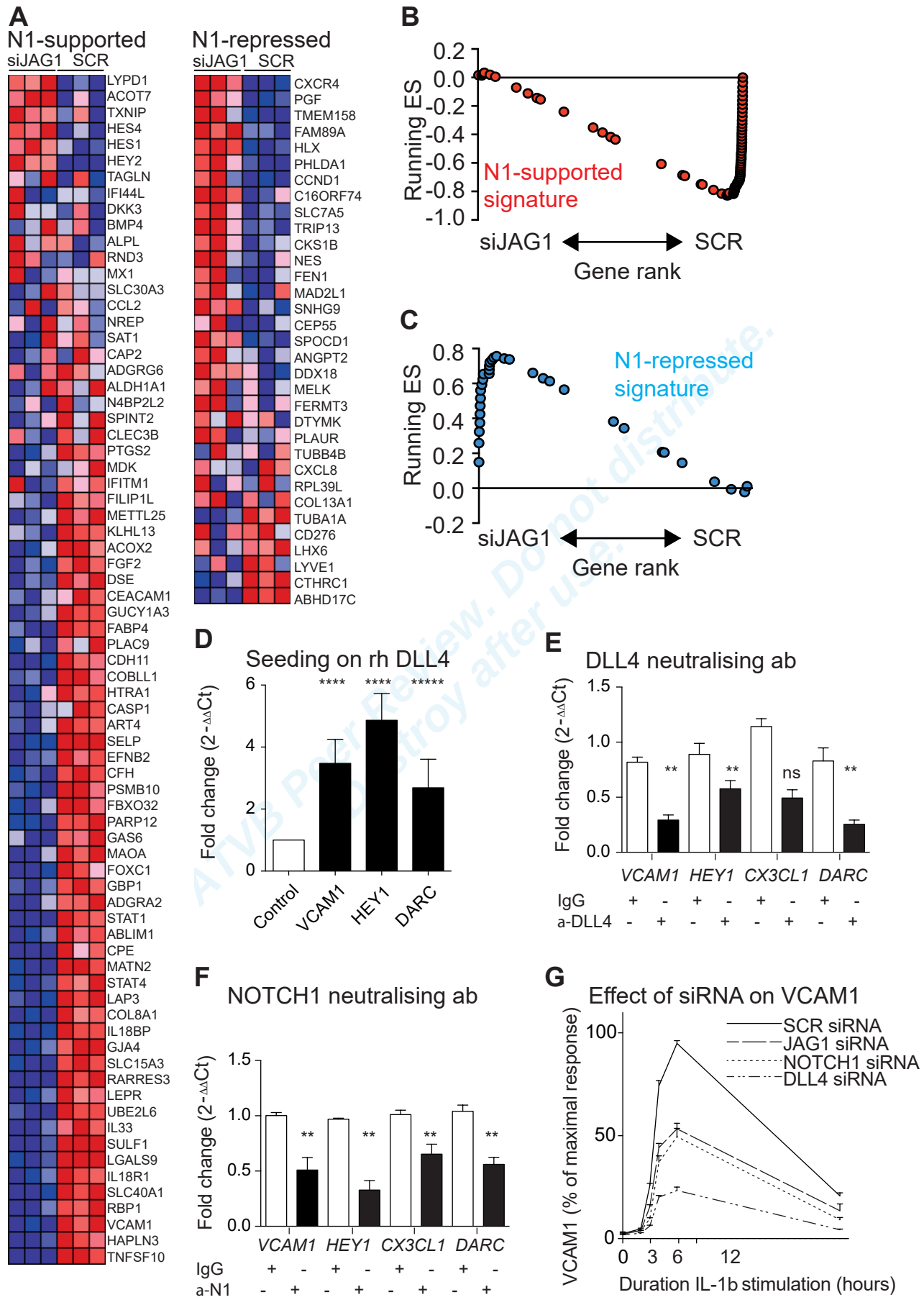

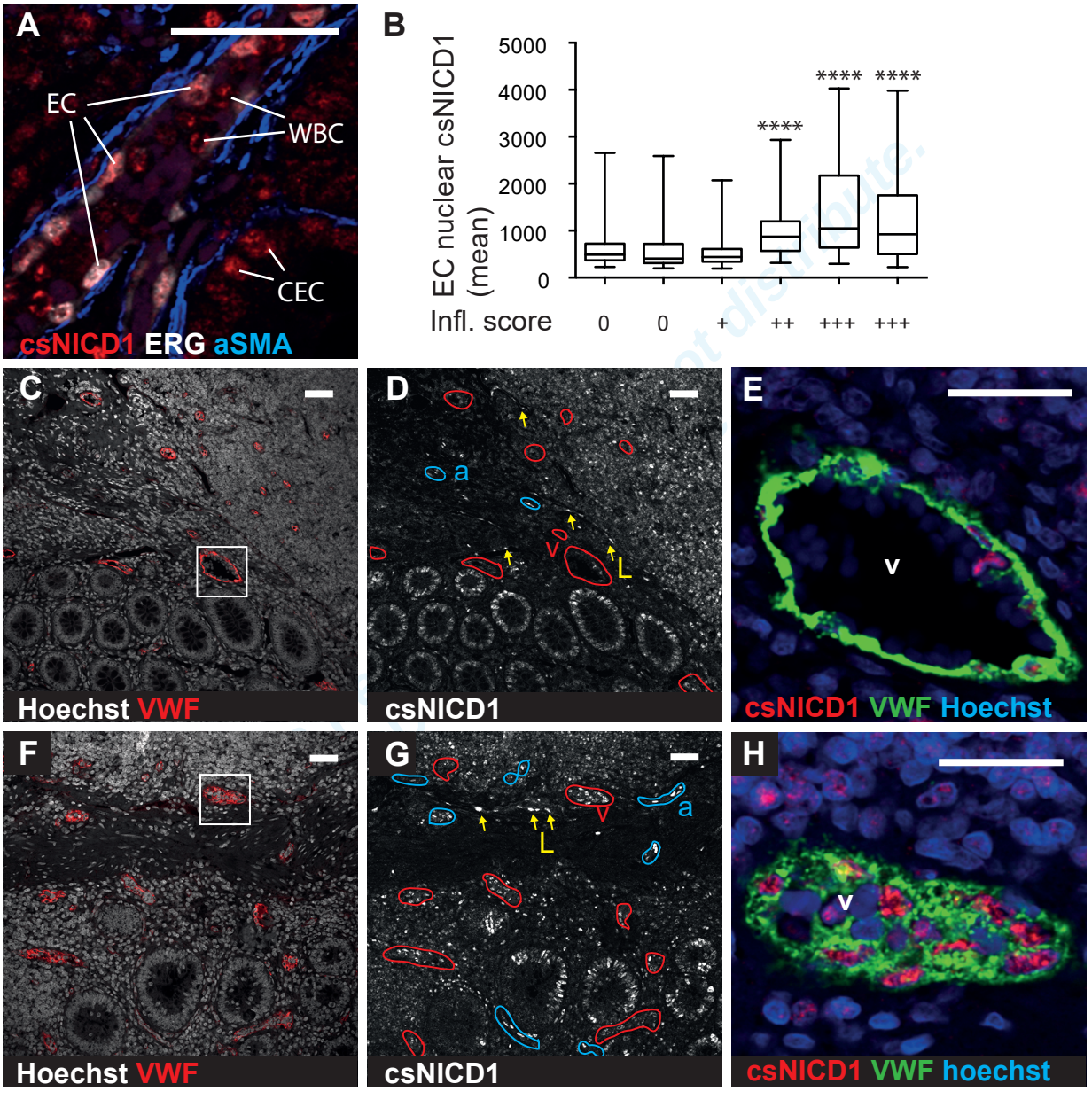
A
EC
WBC
CEC
csNICD1 ERG aSMA
B
EC nuclear csNICD1 (mean)
5000
4000
3000
2000
1000
0
****
****
****
Infl. score
0
0
+
++
+++
+++
C
Hoechst VWF
D
a
V
L
csNICD1
E
v
csNICD1 VWF Hoechst
F
Hoechst VWF
G
L
V
a
csNICD1
H
v
csNICD1 VWF hoechst

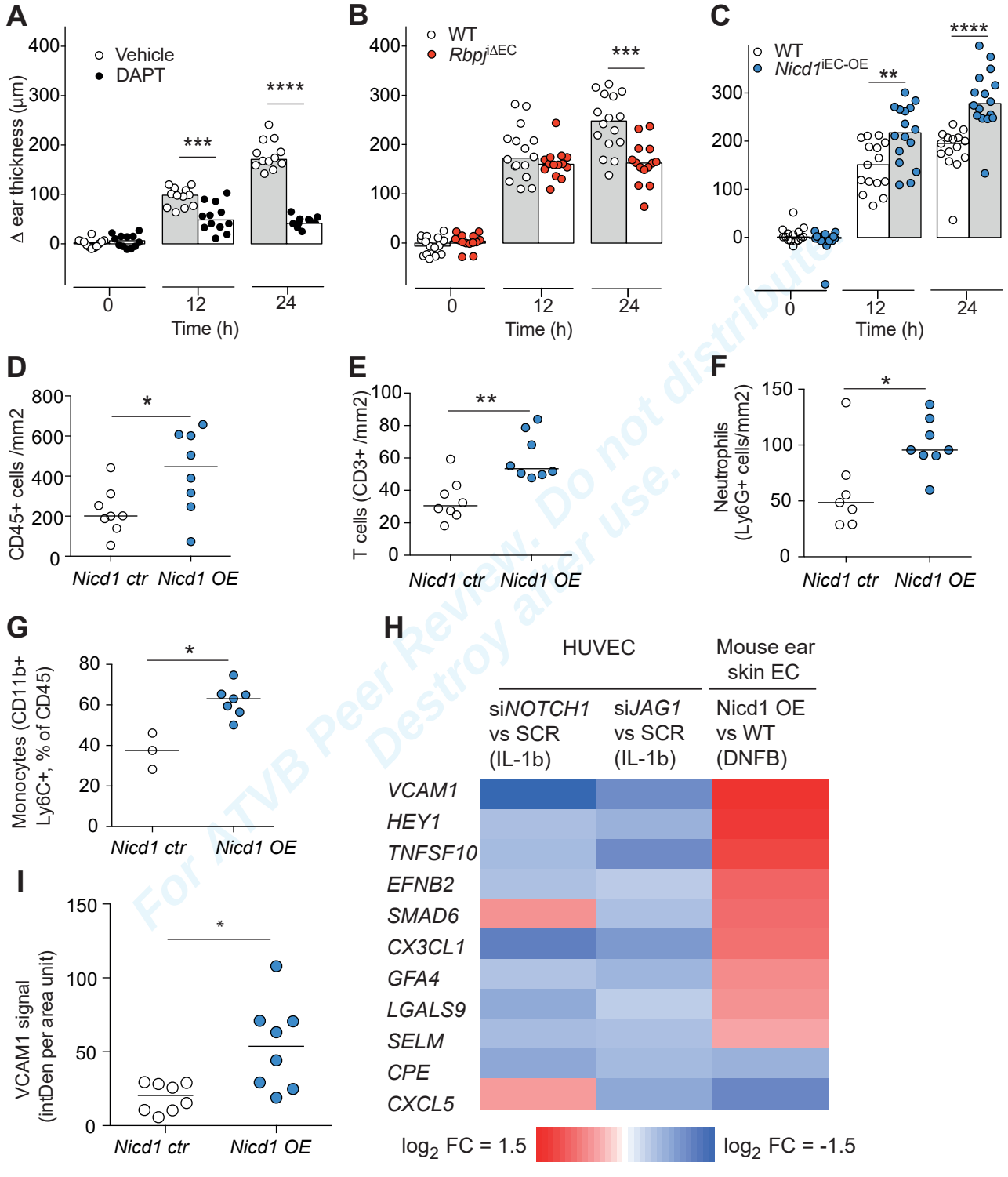

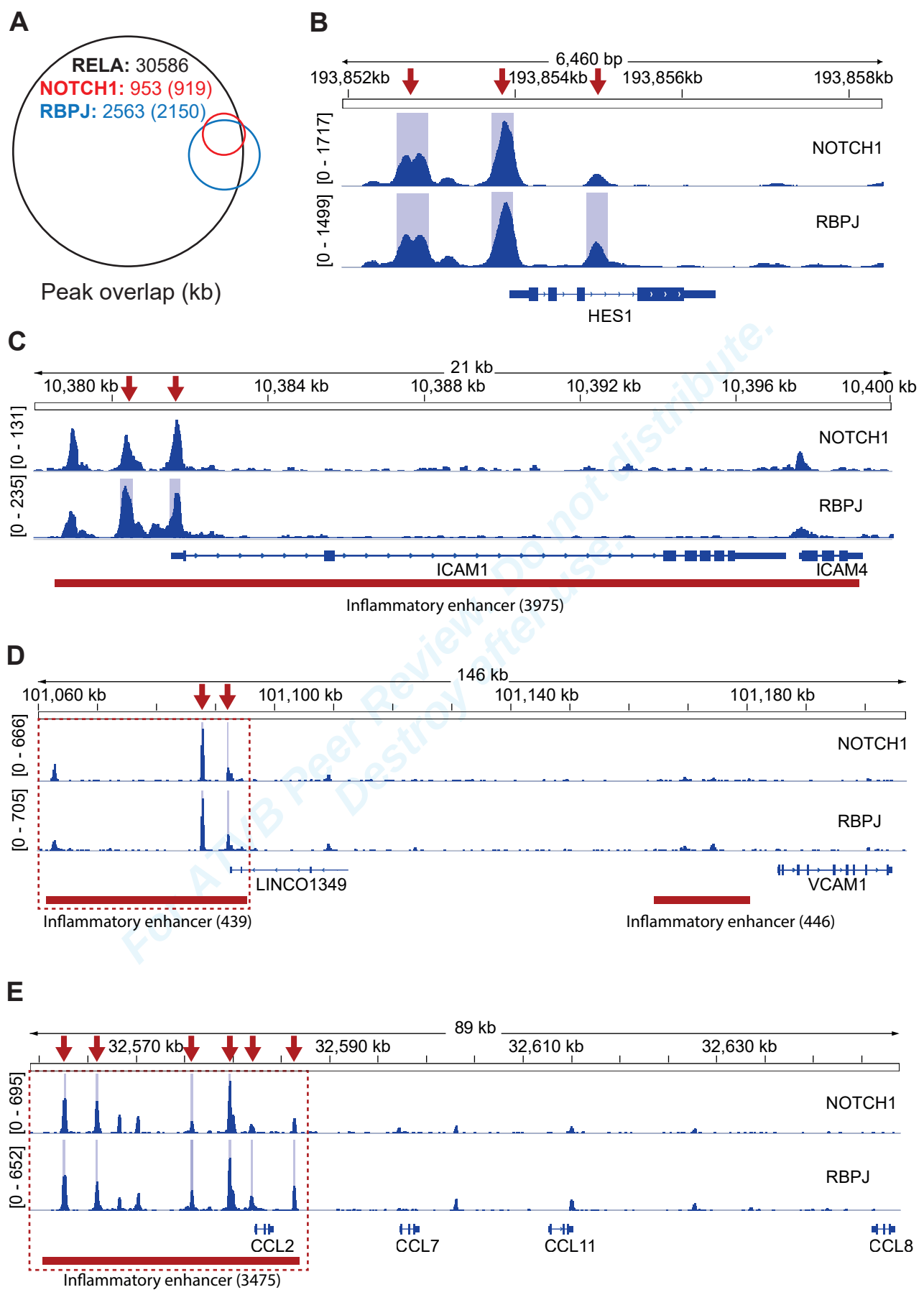

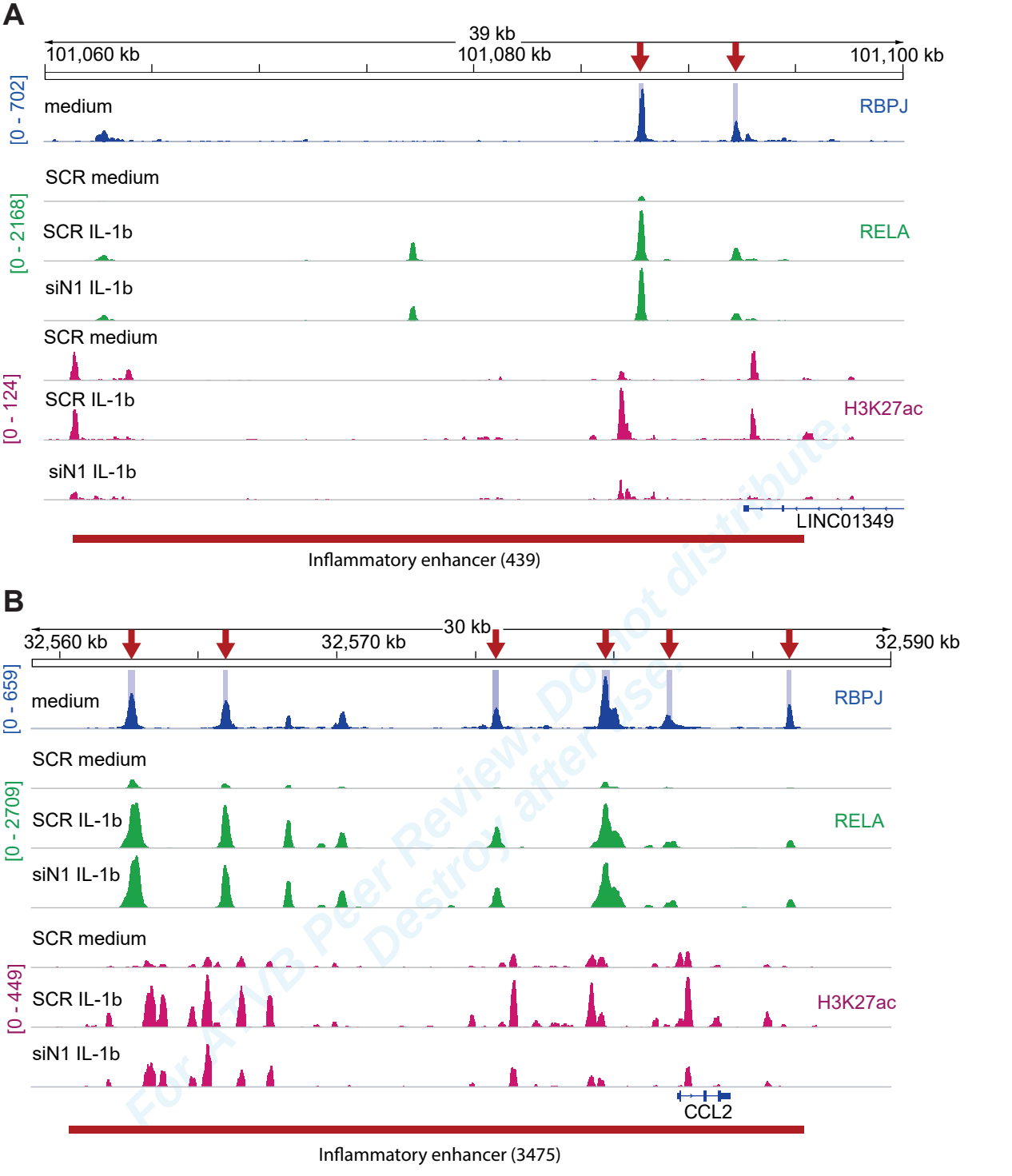

Inhibition of endothelial NOTCH1 signaling attenuates inflammation by reducing cytokine-mediated histone acetylation at inflammatory enhancers

Lars la Cour Poulsen[1,7], Reidunn Jetne Edelmann[1,7], Stig Krüger[1], Rodrigo Diéguez-Hurtado[2], Akshay Shah[4], Tor Espen Stav-Noraas[1], Anastasia Renzi[1], Monika Szymanska[1], Junbai Wang[1], Manuel Ehling[2], Rui Benedito[2], Monika Kasprzycka[1], Espen Bækkevold[1], Olav Sundnes[1], Kim S. Midwood[5], Helge Scott[1], Philippe Collas[4], Christian W. Siebel[6], Ralf H. Adams[2], Guttorm Haraldsen[1,*], Eirik Sundlisæter[1,8], and Johanna Hol[1,8]

[1]Department of Pathology, Oslo University Hospital Rikshospitalet and University of Oslo, 0424 Oslo, Norway
[2]Max Planck Institute for Molecular Biomedicine, Department of Tissue Morphogenesis, University of Münster, 48149 Münster, Germany
[3]Molecular Genetics of Angiogenesis Group, Centro Nacional de Investigaciones Cardiovasculares Carlos III (CNIC), Melchor Fernández Almagro, 3, Madrid, E-28029, Spain
[4]Department of Molecular Medicine, Institute for Basal Medical Sciences, University of Oslo, 0317 Oslo, Norway
[5]The Kennedy Institute of Rheumatology, Nuffield Department of Orthopaedics, Rheumatology and Musculoskeletal Sciences, University of Oxford, Oxford OX3 7FY, UK
[6]Department of Discovery Oncology, Genentech, Inc., South San Francisco, California 94080, USA
[7]Co-first author
[8]Contributed equally to this work

Running title: NOTCH1 inhibition modulates inflammatory enhancers

*Correspondence: Guttorm Haraldsen, Department of Pathology, Oslo University Hospital Rikshospitalet, PO Box 4950 Nydalen, NO-0424 Oslo, Norway. Phone: (+47) 23 07 14 92 Fax: (+47) 23 07 15 11. E-mail: gharalds@rr-research.no

Keywords: Endothelial cell, novel mechanistic insight, inflammation, leukocyte recruitment, transcriptional regulation

Subject codes: Cell Signalling/Signal Transduction, Inflammation, and Vascular Biology

Word count (including figure legends): 7490

Total number of figures and tables: 6 figures, no tables

TOC category: basic

TOC subcategory: Vascular Biology

Summary

Objective: Endothelial upregulation of adhesion molecules serves to recruit leukocytes to inflammatory sites and appears to be promoted by NOTCH1; however, current models based on interactions between active NOTCH1 and NF-κB components cannot explain the transcriptional selectivity exerted by NOTCH1 in this context.

Approach and Results: Observing that Cre/Lox-induced conditional mutations of endothelial Notch modulated inflammation in murine contact hypersensitivity, we found that IL-1β stimulation induced rapid recruitment of RELA to genomic sites occupied by NOTCH1-RBPJ, and that NOTCH1 knockdown reduced H3K27 acetylation at a subset of NF-κB-directed inflammatory enhancers.

Conclusions: Our findings reveal that NOTCH1 signaling supports the expression of a subset of inflammatory genes at the enhancer level and demonstrate how key signaling pathways converge on chromatin to coordinate the transition to an inflammatory endothelial phenotype.

Graphic abstract

Submitted as separate file.

Abbreviations

NICD/NICD1 - NOTCH/NOTCH1 intracellular domain
HUVECs - Human umbilical vein endothelial cells

Introduction

The Notch signaling system coordinates cell differentiation during embryogenesis and postnatal development by linking the fate of one cell with that of its neighbors. To achieve this coordination, mammals have five ligands (Delta-like (DLL)-1, -3, and -4, and Jagged (JAG)-1 and -2) that signal via four Notch receptors (NOTCH 1-4). Such signaling leads to γ-secretase-dependent release of the NOTCH intracellular domain (NICD) and translocation of NICD to the nucleus, where it recruits coactivators and forms an active transcription complex with the transcription factor RBPJ (also known as CBF1, Su(H), Lag1 or CSL)[1,2].

Recent evidence reveals that the Notch pathway is involved in regulation of inflammation. This is not entirely surprising, because NOTCH1 has been found to interact with the NF-κB pathway in cancer[3,4] and therefore has the potential to modulate the actions of proinflammatory cytokines such as TNF (tumor necrosis factor)-α and IL-1 (interleukin-1)-β as well as Toll-like receptor agonists. Indeed, inhibition of Notch signaling ameliorates experimental arthritis[5], acute colitis[6], acute lung injury[7], and graft-versus-host disease[8].

A requirement for effective inflammation is the activation of endothelial cells in postcapillary venules. Vascular upregulation and presentation of adhesion molecules and chemokines direct the sequential recruitment of specific leukocyte subsets, and, while the molecular events involved in leukocyte transmigration have been thoroughly described[9], our understanding of the mechanisms that control the endothelial response to inflammatory activation is still incomplete.

Notably, the role of endothelial Notch signaling in inflammatory activation appears to be highly context-dependent: While hemizygous deletion of endothelial *Notch1* predisposed for atherosclerosis development and monocyte recruitment in the L-sIDOL model[10], endothelial-specific deletion of the canonical Notch transcription factor *Rbpj* in ApoE$^{-/-}$ mice reduced atherosclerotic plaque inflammation and leukocyte recruitment[11]. Notably, NOTCH1 augmented TNF-driven upregulation of the adhesion molecules VCAM1 and ICAM1 in human endothelial cells[12], and endothelial-specific overexpression of active Notch1 in mouse melanoma promoted a proinflammatory, dysfunctional phenotype that included enhanced VCAM1 expression[13]. In contrast, inhibition of NOTCH4 boosted the upregulation of VCAM1 in TNF-stimulated human endothelial cells, suggesting that NOTCH1 and NOTCH4 play opposing roles in the regulation of VCAM1[14]. The effect of NOTCH1 on other classes of inflammatory mediators is, however, less clear-cut, exemplified by the neutrophil-recruiting chemokines CXCL1 and CXCL8 that appear to be repressed by NOTCH1[10,13]. Inflammatory events in endothelial cells are to a large extent driven by NF-κB signaling[15], and it has been suggested that the activated NOTCH1 receptor fragment drives adhesion molecule expression by directly interacting with NF-κB subunits to facilitate their nuclear translocation and retention[11]. However, this mechanism does not account for the apparent selectivity with which NOTCH1 modulates the expression of inflammatory genes in endothelial cells.

A recently identified molecular event of endothelial cell activation is the NF-κB-directed activation of inflammatory enhancer regions, including BRD4-dependent super enhancers essential to the transcriptional inflammatory response[16]. Enhancers have also been identified as the main regions containing functional Notch binding sites that exert transcriptional control over long distances[17,18]. However, it is not known whether Notch associates with inflammatory enhancers or affects inflammation at the genomic level.

We here show that endothelial NOTCH1 signaling promotes leukocyte recruitment by facilitating the activation of inflammatory enhancers supporting a distinct vascular transcription profile. Our findings demonstrate that NOTCH1 signaling is fundamentally involved in regulating the inflammatory response in endothelial cells, supporting the assumption that it may serve as a novel therapeutic target in chronic inflammatory disease.

Materials and methods

Reagents

IL-1β, IFN-γ, TNF-α, epidermal growth factor (EGF), and basic fibroblast growth factor (bFGF) were from R&D Systems; hydrocortisone and dinitrofluorobenzene (DNFB) from Sigma Aldrich; fetal bovine serum (FBS), gentamicin, fungizone, L-glutamine, MCBD 131, Opti-MEM and TRI Reagent from Thermo Fisher Scientific, trypsin-EDTA from BioWhittaker, and the γ-secretase inhibitor N-[N-(3,5-difluorophenacetyl)-l-alanyl]-S-phenylglycine t-butyl ester (DAPT) from EMD Chemicals.

Cell culture

Umbilical cords were obtained from the Department of Gynecology and Obstetrics at Oslo University Hospital according to a protocol approved by the Regional Committee for Research Ethics, Health Region South, Norway (2014/298 S-05152a). Human umbilical vein endothelial cells (HUVECs) were isolated as previously described [19] and cultured on 0.1% gelatine-coated plastic in MCBD 131 medium containing 7.5% FBS, 10 ng/mL EGF, 1 ng/mL bFGF, 1 µg/mL hydrocortisone, 50 µg/mL gentamicin, 250 ng/mL fungizone, and 1% L-glutamine. Cells were maintained at 37°C in 95% humidity/5% CO_2 atmosphere, split 1:3, and used at passage 2-6.

Human biopsy material

Formalin-fixed, paraffin-embedded (FFPE) samples of human appendix (appendicitis n=4, control n=2) were obtained from the diagnostic biobank at the Division of Pathology, Oslo University Hospital, and used in accordance with a protocol approved by the Regional Committee for Research Ethics, Health Region South, Norway (2014/298 S-05152a). Biopsies were scored by a senior clinical pathologist according to the degree of inflammation in the lamina propria as follows: evidence of granulocyte infiltration (+); granulocyte infiltration and loss of crypts (++); and when also including ulceration/ necrosis (+++).

Immunostainings and microscopy

All antibodies for immunostainings and working concentrations are specified in the online-only Major Resource Table. CD45 was detected by manual staining: Tissue sections (4 µm thick, FFPE) were deparaffinized, boiled for 20 min in DAKO target retrieval buffer pH 6.1, incubated with 5% donkey serum for 30 min at room temperature, incubated with primary antibodies diluted in PBS with 1.25% BSA overnight at 4°C, and then incubated with fluorescently labeled secondary antibodies for 60 min at 37°C. Hoechst 33258 nuclear dye (0.5 µg/mL) was used as counterstain. csNICD1, Ly6G and CD3 were detected using the automated Ventana Discovery Ultra system, using standard deparaffinisation, 80 min antigen retrieval in CC1 buffer, Disc inhibitor 4 min (CD3) or 8 min (csNICD1), incubation with primary antibody (60 min), rabbit antibody amplification (csNICD1), rabbit anti-rat-FC (clone R18-2, abcam, Ly6G only), UltraMap anti-rabbit-AP (CD3, 8 min) or UltraMap anti-rabbit-HRP (csNICD1, 20 min) followed by incubation with Fast Red (Ly6G, CD3) or rhodamine (csNICD1, 12 min). Ventana Discovery protocols are available upon request. All reagents for automatic staining were purchased from Roche. Slides were washed in warm, soapy water and either mounted at this point or incubated with primary antibodies targeting vascular markers diluted in PBS with 1.25% BSA overnight at 4°C, proceeding with further manual staining as described above. Slides were mounted in ProLong Diamond Antifade mountant (Thermofisher). Irrelevant, concentration-matched primary antibodies were used as negative controls.

Confocal microscopy was performed using an Olympus FV1000 confocal microscope with 20x UPlanApo N.A. 0.80 and 60x UPlanSApo N.A. 1.35 objectives. Images were obtained using the Olympus Cell P (Olympus, Tokyo, Japan) image acquisition software. ImageJ v2.0.0-rc-41/1.50b and Adobe Photoshop CS6 v13.0 x64 (Adobe Systems, San Jose, CA) were used to adjust brightness and contrast, always applying identical settings to specific staining and controls. Light microscopy images were obtained using an Olympus BX51

Formatted: Left

Formatted: Left

Formatted: Left

microscope with an Olympus U-TVO.5XC camera and Olympus CellR^ image acquisition software.

Image analysis

Dermal CD3 positive cells and Ly6G positive cells were counted manually from images obtained by scanning whole sections of DNFB-treated ears using a Pannoramic Midi scanner (3D Histiotech). Images were coded and counted blindfolded. Automated image analysis of csNICD1, CD45 positive cells, and VCAM1 was performed in Image J (v2.9.9-rc-41/1.50b). Endothelial csNICD1 signal was quantified in 10 high power (x60) confocal images per patient, typically including 100-200 endothelial nuclei in total per patient. The channel depicting ERG was used to define each endothelial nucleus as a separate region of interest (ROI), and the mean signal intensity in the channel depicting csNICD1 was measured for each ROI. CD45 positive cells were counted automatically from merged images (n=8 per group) obtained using a Zeiss Axioscan Z1 slide scanner with filter sets 38 HE and 49 and analyzed using the Measure>Analyze particle function in ImageJ. Blinded automatic quantification of VCAM1 signal was performed using five x20-fields from each DNFB treated ear (n=8 mice per group). The region from the middle of the cartilage of the pinna to the inner epidermal border was selected manually using the ROI tool. Autofluorescent noise was reduced by subtracting 25 arbitrary units from the fluorescent signal. Integrated Density values (representing the product of number of pixels measured and the mean grey value per pixel) were normalized using the ratio between measured area in that section to the mean area of all sections measured. As edema is mainly confined to one side of the pinna, VCAM1 signal was measured on the opposite side, thus allowing similarly sized ROIs between the different mice.

Formatted: Left

Knockdown experiments

Silencer select predesigned siRNAs for *JAG1*, *DLL4, NOTCH1,* negative controls, and transfection reagents were obtained from Thermo Fisher Scientific. Initial transfections (Figure 1) were performed on HUVECs in suspension incubated with a precomplexed mixture of siPORT amine transfection agent and 40 nM siRNA oligonucleotides in Opti-MEM and plated at a density of 7.2×10^4 cells/cm^2. The protocol was later optimized and HUVECs were instead plated 3×10^4 cells/cm^2 and transfected the next day using Lipofectamine RNAimax and 27 nM siRNA. The medium was replaced by regular growth medium after 6 hours. Unless otherwise stated, IL-1β was added at 5 ng/ml 48 hours post transfection and the cultures were incubated for the indicated time.

Formatted: Left

***In vitro* stimulation and blocking of Notch signaling**

For immobilization of JAG1 and DLL4, six-well culture plates (Corning Inc) were first incubated with goat polyclonal anti-human IgG (I3382, 6.48 µg/ml, R&D Systems) or rabbit polyclonal anti-His (A00174, 6.48 µg/ml, GenScript) as described previously [20] and then with recombinant JAG1-Fc (1277-JG, 2.47 µg/ml, R&D Systems) or DLL4-His (1506-D4, 1 µg/ml, R&D Systems), respectively. rhIgG$_1$-Fc or BSA were used as controls. HUVECs were seeded at $2.5\text{x}10^4$ cells/cm^2 and harvested after 24-48 hours.

Formatted: Left

All antibodies used for *in vitro* blocking of JAG1, Dll4 and NOTCH1 in HUVECs and respective working concentrations are specified in the online-only Major Resource Tables. Species-, isotype-, and concentration-matched monoclonal antibodies against the E-tag peptide (clone 73009, R&D Systems), KLH (clone 11711, R&D Systems), *Aspergillus niger* glucose oxidase (clone DAK-GO1, DakoCytomation) or human IgG1 (Genentech) were used as negative controls. Antibodies were added to the culture one hour prior to the addition of IL-1β.

Cellular fractionation and transcription factor DNA-binding ELISA

HUVECs were fractionated into nuclear extract and cytoplasmic extracts by the Nuclear Extract Kit from Active Motif. When used for Western blotting, a 6xSDS buffer was added to the extracts to match the Western blotting conditions described below. The DNA binding

Formatted: Left

potential of nuclear RELA, p50, cFOS, and phosphorylated cJUN (Ser73) was measured by the TransAM Transcription Factor ELISA kits from Active Motif.

Protein extraction and Western Blot

Cells were washed twice in PBS before lysis in an SDS buffer (2% SDS, 50 mM Tris-HCl, 10% glycerol, 0.08% bromophenol blue, 100 mM β-mercaptoethanol, Complete Protease and PhosStop Phosphatase inhibitor cocktails from Roche) to prepare whole cell extracts. Protein concentrations were determined by the RC DC Protein Assay from Bio-Rad.

Protein extraction from samples used for microarray analysis was done from the organic phase of TRI Reagent samples as previously described [21]. The dialysate was centrifuged and the clear supernatant was concentrated 10-fold in Vivaspin sample concentrators (Sartorius AG). Protein concentration was determined on the Nanodrop ND-1000 Spectrophotometer (Thermo Scientific). Western blotting was performed on equal protein amounts (10-20 µg) by a Bio-Rad workflow (Mini-PROTEAN TGX Precast Gel, Trans-Blot Turbo Transfer System with Nitrocellulose Transfer Packs, and ChemiDoc MP System) with the exception that the SuperSignal West Dura substrate from Thermo Fisher Scientific was used for ECL-detection. 5% Blotting-Grade Blocker (Bio-Rad) in TBS with 1% Tween 20 (TBST) was applied for membrane blocking except for phospho-protein detection where 5% BSA was used. Membranes were incubated with primary antibodies at 4°C overnight, followed by HRP-linked secondary antibody, 1 hour at room temperature. HRP signal was detected by chemiluminescence (substrate 32106 or 34076, Pierce, Thermo Scientific) and analyzed on a Kodak Image Station 4000R. All primary antibodies used for Western blot are listed in the online-only Major Resource Tables.

Cellular Enzyme-Linked Immuno-Sorbent Assay (CELISA)

Total cellular expression of VCAM1 was quantified by CELISA on fixed, adherent HUVECs as previously described [22].

Flow cytometry

Single-cell suspensions obtained by gentle EDTA treatment (~10 min; 5 µM in PBS) of HUVECs were incubated on ice (30 min) with primary antibodies specified in in the online-only Major Resource Tables followed by R-phycoerythrin-labelled goat anti-mouse IgG_1 conjugate (1072-09, 2 µg/ml, Southern Biotech) for 20 min. The final suspension was made in medium containing TO-PRO®-3 iodide (1 µM, Life Technologies). An irrelevant isotype- and concentration-matched primary antibody served as control. The samples were analyzed on a fluorescence-activated cell sorter (FACScalibur, Becton Dickinson). For quantification of leukocytes from mouse ears, cell suspensions were obtained as described below ("Collection and sorting of mouse endothelial cells") and CD45+ cells were incubated on ice (30 min) with antibodies as specified in the online-only Major Resource Tables. The samples were analyzed on a fluorescence-activated cell sorter (FACSAria II, Becton Dickinson).

Gene-expression profiling and Gene Ontology Analysis

Total RNA was isolated using the RNeasy Mini or Micro Kits (Qiagen) as recommended by the manufacturer. Human gene expression profiles were obtained by Illumina HumanHT-12 v4 Expression BeadChips and mouse expression profiles by Affymetrix Mouse Gene ST 2.1 Arrays. Data has been deposited as a super series in NCBI's Gene Expression Omnibus [23] and are accessible through GEO accession number GSE85987. Raw data was imported into R (version 3.3.0)/Bioconductor/Beadarray [24] (Illumina) or Oligo [25] (Affymetrix) and quantile (human) or RMA (mouse) normalized. Differentially expressed genes were identified by using the moderated t approach in R/Bioconductor/Limma [26]. The Benjamini-Hochberg´s method was used to control the false discovery rates. Gene Ontology analysis [27] was performed using the GO Consortium database (version released 20160822) and the Panther overrepresentation test (version released 20160715).

Real-time quantitative RT-PCR (RT-qPCR)

For real-time RT-qPCR, HUVECs were lysed directly in the culture dish with TRI Reagent. Total RNA was isolated using the RNeasy Mini Kit (Qiagen) according to the manufacturer´s

Formatted: Left

Formatted: Left

Formatted: Left

Field Code Changed

Formatted: Left

instructions. RNA was reverse-transcribed using Oligo(dT) and Superscript III reverse transcriptase (Life Technologies). Gene transcripts were quantified using the Mx3000P system (Agilent Technologies), normalized against hypoxanthine-guanine phosphoribosyl transferase (HPRT), and fold changes calculated according to the comparative C_T method [28]. Sequences of qPCR primers used in this study are given in in the online-only Major Resource Tables.

ChIP-seq

Chromatin immunoprecipitation (ChIP) combined with deep sequencing (ChIP-seq) was performed on pools of HUVECs from 13 donors grown on 15 cm^2 culture dishes. Cells used for NOTCH1 and RBPJ ChIP-seq were cultured 48 hours beyond reaching confluence to induce quiescence [29] before crosslinking and harvest. Cells used for RELA and H3K27ac ChIP-seq were transfected with *NOTCH1* or Scr siRNA 60 hours before stimulation with IL-1β for 1 hour. Knockdown efficiency was assessed by Western blotting in parallel experiments. Chromatin immunoprecipitation (ChIP) for RELA, NOTCH1 and RBPJ was performed on HUVECs as previously described [16] with the exception that a two-step crosslinking procedure (45 min in 2 mM di-succinimidyl glutarate (DSG) followed by 10 min in 1% formaldehyde (FA) and quenching in 125 mM glycine) [30] and longer sonication (24 cycles of 30 sec ON/OFF at high intensity at the Bioruptor Twin) were applied. For H3K27ac ChIP-seq, only 10 min FA crosslinking was applied. Cells were lysed in 1.6 mL lysis buffer (0.1% SDS, 1% Triton X-100, 0.15 M NaCl, 1 mM EDTA, 20 mM Tris pH 8), removed with a cell scraper, and kept at 4°C (NOTCH1 and RBPJ) or -80°C (RELA and H3K27ac) before sonication. DSG/FA and FA samples were sonicated for 40 or 16 cycles, respectively, as described for ChIP-qPCR. To remove cell debris, samples were centrifuged at 10,000g for 1 min. Immunoprecipitation was performed in 15 mL tubes containing $1.5x10^7$ cells in a final volume of 6 mL lysis buffer with 1 mg/mL BSA. Chromatin was incubated with antibodies (see the online-only Major Resource Tables) for 3 hours at 4°C with upside-down rotation. Protein A sepharose beads (150 µL per ChIP-seq washed thrice in lysis buffer and resuspended in a final of 750 µL lysis buffer with 750 µg BSA) were added and samples were incubated overnight at 4°C with upside-down rotation. Beads were washed in 12 mL wash buffers as follows: 2x wash buffer 1 (0.1% SDS, 0.1% NaDOC, 1% Triton X-100, 0.15 M NaCl, 1 mM EDTA, 20 mM HEPES), 1x wash buffer 2 (0.1% SDS, 0.1% NaDOC, 1% Triton X-100, 0.5 M NaCl, 1 mM EDTA, 20 mM HEPES), 1x wash buffer 3 (0.25 M LiCl, 0.5% NaDOC, 0.5% NP-40, 1 mM EDTA, 20 mM HEPES), and 2x wash buffer 4 (1 mM EDTA, 20 mM HEPES), before treatment with RNase A (100 microgram/mL) in water for 20 min at 37°C and elution in 2x200 µL buffer (0.1M NaHCO3, 1% SDS) for 2x15 min at room temperature with upside-down rotation. Samples were then treated with 60 µg Proteinase K for 1 hour at 55°C and subjected to decrosslinking in 300 mM NaCl by overnight incubation at 65°C. DNA was purified by standard PCI/chloroform extraction and ethanol precipitation and resuspended in 60 µL water. For input samples, 0.7% sonicated material was processed in parallel to the ChIP-seq samples from the RNase-treatment step. Chromatin shearing was assessed by agarose gel electrophoresis and ChIP-seq quality was tested by ChIP-qPCR. DNA concentration was determined by the Quant-iT PicoGreen dsDNA assay kit from Life Technologies. 10 ng samples were used for library preparation by the Illumina sample preparation kit before sequencing on Illumina Hiseq4000 (RBPJ, NOTCH1) or Illumina Nextseq500 (RELA, H3K27ac) instruments.

ChIP-seq analysis

Samples were sequenced on an Illumina Hiseq4000 (RBPJ, NOTCH1) or Illumina Nextseq500 (RELA, H3K27ac) machine as described above. Fastq files were mapped to hg19 reference genome from Illumina iGenomes database, using bowtie [31]. Some samples were sequenced as paired-end 151 bp reads (RBPJ, NOTCH1) and some as single-end 75 bp reads (RELA, H3K27ac). Paired-end sequences overlapped their respective mates in genomic position. Thus, only one mate was used for the paired-end samples. Duplicate reads were filtered out using the rmdup function from SAMtools suite [32]. Data was converted to bigWig format and viewed in the Integrative Genomics viewer to generate screenshots [33].

Formatted: Left

Field Code Changed

Peak calling was performed using callpeak function from macs2 [34]. Peaks overlap data was generated by using multiinter function of the BEDTools suite [35]. Base-pair overlap was calculated by a custom Perl script which counted the number of bases in each intersect. Average profiles were generated by using ngs.plot.r [36] and replotted in R [37] with ggplot [38]. All NOTCH1 peaks were used for average profile enrichment around NOTCH1 peaks. For RELA average profiles, all peaks were combined and common regions were merged using merge function from BEDTools suite. Endothelial superenhancer (SE) regions were obtained from reference [16] and lifted to hg19. TNF-induced SEs overlapping with NOTCH1 peaks were identified and base pair overlaps with H3K27ac peaks in the IL-1β-stimulated samples with or without *NOTCH1* knockdown were determined as above.

Field Code Changed

Mice

Mouse strains used are described in the online-only Major Resource Tables. Genotyping was performed as previously described [39]. To trigger Cre-mediated gene inactivation (*Rbpj*) or homozygous constitutive activation (*NICD*) in postnatal mice, intraperitoneal injections of 1 mg tamoxifen (Sigma T5648) dissolved in a mixture of ethanol, polyethoxylated castor oil (Kolliphor EL, BASF Corp.) and PBS 1:1:8, were given daily for 5 consecutive days, starting 6 days before sensitization with dinitrofluorobenzene (DNFB) unless indicated otherwise. The specificity and efficiency of Cre activity were verified by reporter lines. Pharmacological inhibition of Notch signaling via DAPT *in vivo* was carried out in 11 weeks old female C57BL6/JBomTac mice. Subsequent experiments were performed in transgenic animals of both sexes, 5-14 weeks old. Animals were matched according to sex and age, and the effects of Notch-modulation were similar in females and males. Transgenic animals of both sexes, 9-11 weeks old, were used for isolation of endothelial cells for transcriptome analysis. A total of 161 mice were used in this study. Power analysis was used to estimate the number of animals required per treatment group. Randomization of treatment groups was not performed. Operators were blinded to the genotype in animal experiments shown in Figure 4. All experiments involving animals were performed according to institutional guidelines and laws, following protocols approved by local animal ethics committees.

Formatted: Left

Murine contact hypersensitivity model

DNFB-induced contact hypersensitivity (Figure IIIA in the online-only Data Supplement) is a delayed type hypersensitivity model for human allergic contact dermatitis. Mice were sensitized to DNFB by painting the shaved abdomen with 25 µl of a 0.5% solution in acetone/olive oil (4:1), in addition to 5 µl to each paw, on day 0 and 1. For systemic inhibition of Notch signaling, 100 mg/kg DAPT dissolved in 10% ethanol and 90% corn oil was administered subcutaneously caudally on the back (injection volume 10 µl/g body weight) 3 hours before ear challenge on day 5. Control mice were injected with vehicle only. On day 5, the elicitation phase was induced by painting the right ear with 20 µl of 0.5% DNFB solution. The thickness of the ears was measured using a micrometer. Swelling was calculated by subtracting the baseline thickness from the thickness measured at various time points. Anesthesia was induced by intraperitoneal injection of xylazine (10mg/kg) and ketamine (100mg/kg) or isoflurane inhalation. No animals were excluded from analysis.

Formatted: Left

Isolation of RNA from mouse ear endothelial cells

Mouse ears were collected and washed in sterile PBS, hair was removed and the ears were minced thoroughly using two scalpel blades. Minced tissue was transferred to 1% Collagenase I dissolved in pre-warmed 5% BSA-PBS, and incubated 2 hours at 37°C on a horizontal shaker. DNAse I was added the last 30 min of incubation. Finally, to obtain a single-cell suspension, samples were passed through a 50 µm cell strainer and washed thrice in FACS buffer (2% FCS, 2 mM EDTA in PBS). Endothelial cells were then sorted in a FACSAria II, directly into RLT buffer, as a CD45-/Ter119-/CD31+ subpopulation with antibodies specified in the online-only Major Resource Tables. The samples were kept at -80°C until RNA was extracted using the Qiagen RNEasy Plus Micro kit. The RNA amount and integrity were assessed using RNA 6000 Pico Kit (Agilent Technologies) in a 2100 Bioanalyzer (Agilent Technologies); Only RNA samples with RIN values>7 were used for

Formatted: Left

downstream microarray analysis. Samples were transported on dry ice to a commercial provider where they were amplified using the Affymetrix WT Pico Amplification kit and hybridized on the Affymetrix Gene Chip Mouse Gene 2.1 ST Array.

Statistical analysis

Statistical analyses were performed using Mann Whitney test, Wilcoxon signed rank test, or Kruskall Wallis followed by Dunn´s multiple comparison test, all in GraphPad Prism (version 6.0h). Because most sample sizes were too small to ensure normal distribution of data, we chose to use nonparametric statistical tests. Microarray data were analyzed using R/Bioconductor/Limma[26] by the moderated t approach and Benjamini-Hochberg's adjustment for multiple comparisons.

~~Materials and Methods are available in the online-only Data Supplement.~~

Field Code Changed

Formatted: Norwegian (Bokmål)

Results

Proinflammatory cytokines selectively drive JAG1 expression in endothelial cells

Endothelial *JAG1* is upregulated by TNF-α via activation of NF-κB and AP-1[40,19]. We therefore assessed the proinflammatory responsiveness of all endothelial Notch ligands in human umbilical vein endothelial cells (HUVECs), observing that the response was restricted to *JAG1,* and that IL-1β, compared to TNF-α, induced an even stronger upregulation of *JAG1* mRNA (Figure 1A). In addition, IFN-γ also gave a moderate response (Figure 1A). At the protein level, cell surface expression of JAG1 was upregulated by IL-1β in a dose- and time-dependent manner, peaking at 5 ng/ml and 12 hours, respectively (Figures IA and IB in the online-only Data Supplement).

JAG1 promotes inflammatory gene expression in endothelial cells

To address whether JAG1 plays a role in inflammatory activation of endothelial cells, we next performed genome-wide transcriptome analysis of IL-1β-stimulated HUVECs treated with siRNA targeting *JAG1* or scrambled siRNA, identifying 135 differentially expressed genes in IL-1β-stimulated cells (Fold change>1.5, Benjamini-Hochberg´s adj.p<0.05; Figure IC in the online-only Data Supplement, genes listed in Table I in the online-only Data Supplement). Gene ontology analysis revealed that genes supported by *JAG1* in IL-1β-stimulated cells were enriched for biological terms associated with leukocyte recruitment (chemokine-mediated signaling pathway, positive regulation of leukocyte chemotaxis), response to proinflammatory stimuli (IFN-gamma-mediated signaling pathway, cellular response to IL-1, cellular response to TNF, response to lipopolysaccharide, response to virus), and inflammatory activation (immune effector process, inflammatory response) (Figure 1B, Table II in the online-only Data Supplement). In contrast, genes repressed by JAG1 in IL-1β-stimulated cells were enriched for biological terms associated with hypoxia and apoptosis (Figure 1B, Table III in the online-only Data Supplement). Interestingly, while knockdown of *JAG1* markedly inhibited the expression of selectins (*SELE*, *SELP*) and adhesion molecules (*VCAM1* and *ICAM1*) in IL-1β-stimulated HUVECs, the effect on chemokines and associated molecules was much more variable, with some being markedly reduced (*DARC*, *CCL8, CX3CL1*) while others remained unaffected (*CXCL8*, *CCL2*) (Figure 1C).

Results were validated by means of RT-qPCR (Figure ID in the online-only Data Supplement). The modulation of VCAM1, CX3CL1, and DARC after *JAG1* knockdown was confirmed at the protein level by flow cytometry (Figure 1D and Figure IE in the online-only Data Supplement). To corroborate the specificity of the knockdown, we also inhibited the function of JAG1 in IL-1β-stimulated cells by means of a neutralizing antibody, observing modulation of target transcripts similar to that observed in response to siRNA treatment (Figure 1E). Furthermore, we inverted the experiment by seeding cells on immobilized recombinant JAG1 in the absence of proinflammatory cytokines, observing enhanced expression of target genes (Figure 1F). It should, however, be noted that *JAG1* siRNA did

not inhibit the expression of inflammatory transcripts in the absence of IL-1β-stimulation (Table IV in the online-only Data Supplement).

Altogether, these results show that inhibition of endothelial JAG1 attenuates the upregulation of a subset of inflammatory mediators with established roles in leukocyte recruitment.

JAG1 maintains expression of NOTCH1-supported genes in activated endothelial cells
Considering the dynamic and competitive balance between JAG1 and DLL4 during angiogenic sprouting[20,20], and the suggested role of JAG1 in priming endothelial cells for angiogenesis after inflammatory activation[41,21], we next asked if JAG1 reinforced or inhibited the expression of NOTCH1-supported genes in IL-1β-stimulated HUVECs. Comparing transcriptome data from confluent HUVECs treated with siRNA targeting NOTCH1 to two published data sets investigating the effect of inhibiting of overexpressing NOTCH1 in cultured human endothelial cells[10,42,10,22], we compiled lists of genes supported or repressed by NOTCH1 in at least two of the three data sets (Figure 2A). Gene set enrichment analysis showed that *JAG1* knockdown mediated negative enrichment of NOTCH1-supported genes (Figures 2A and 2B) and positive enrichment of NOTCH1-repressed genes (Figures 2A and 2C) in IL-1β-stimulated HUVECs.

JAG1 inhibition is mirrored by targeting DLL4 or NOTCH1
HUVECs seeded on immobilized recombinant DLL4 substantially increased their expression of *VCAM1* and *DARC* (Figure 2D), and inhibition of DLL4 by a neutralizing antibody reduced the IL-1β-induced transcription of *VCAM1*, *DARC,* and *CX3CL1* in a similar manner to JAG1 inhibition (Figure 2E). Moreover, administration of a neutralizing antibody against NOTCH1 reduced the IL-1β-induced expression of *VCAM1*, *DARC,* and *CX3CL1* (Figure 2F). Finally, siRNA-mediated knockdown of *NOTCH1, JAG1,* or *DLL4* inhibited VCAM1 protein expression as detected by a cell-based ELISA assay (Figure 2G). Notably, and despite the marked increase in JAG1 expression during inflammatory activation, *JAG1*, *DLL4* and *NOTCH1* knockdown all attenuated VCAM1 induction with similar kinetics. It should also be noted that the effect of IL-1β on NOTCH1-supported genes was diverse (Figure II in the online-only Data Supplement), with some genes (e.g. *FABP4*, *FOXC1*) being induced and others (e.g. *HES1*, *HES4*, *IL33*) being repressed by inflammatory activation.

Taken together, these data show that JAG1, DLL4, and NOTCH1 all support the upregulation of a similar subset of inflammatory mediators in cultured human endothelial cells and confirm previous observations that the cytokine-induced upregulation of JAG1 serves to maintain NOTCH1 signaling under inflammatory conditions.

NOTCH1 is activated in endothelial cells of inflamed human appendix
Considering that NOTCH1 signaling supported the upregulation of leukocyte-recruiting factors *in vitro*, we next asked if active NOTCH1 could be observed in endothelial cells of inflamed human tissues. When immunostaining biopsies with an antibody that recognizes the intracellular domain of human NOTCH1 only when released by cleavage before Val1754[43,23] (csNICD1), we observed strong csNICD1 signal in endothelial cells of a subset of vessels in inflamed appendix (Figure 3A). Endothelial identity was confirmed by co-staining with the endothelial-specific transcription factor ERG. We next quantified the nuclear csNICD1 signal in lamina propria endothelial cells (ERG positive) and observed significantly higher levels of csNICD1 in biopsies with moderate to severe inflammation (scores ++ or +++) than in biopsies with no or little inflammation (scores 0 or +) (Figure 3B).

Because leukocyte recruitment takes place at the level of post-capillary venules, we next mapped the endothelial csNICD1 signal in different branches of the vascular tree. To this end, we used morphological criteria and a panel of molecular markers (detailed in Table V in the online-only Data Supplement) to identify arterioles, venules, capillaries, and lymphatic vessels. In noninflamed control specimens (Figures 3C, 3D, and 3E), we observed a strong nuclear signal for csNICD1 in endothelial cells of arteriolar and lymphatic vessels (VE-cadherin-positive, VWF-negative, sparse cytoplasm, absence of aSMA-positive perivascular

cells), while the majority of mucosal and submucosal venular endothelial cells (positive for the postcapillary venule-specific marker DARC[44][24], not shown) were negative or only weakly positive for csNICD1 under matching conditions for staining and exposure (Figures 3D and 3E, labelled a, L and v, respectively). By contrast, postcapillary venules of inflamed specimens (Figures 3F, 3G, and 3H, labelled v) altogether showed an induction of nuclear endothelial signal for csNICD1 at the mucosal-submucosal border. Together, these findings suggest that endothelial NOTCH1 signaling in the gastrointestinal tract is subject to spatial and temporal regulation in the context of inflammation.

Notch signaling modulates the contact hypersensitivity response

To evaluate the functional importance of our observations, we used the DNFB-induced contact hypersensitivity model (Figure IIIA in the online-only Data Supplement). We observed that subcutaneous injection of the γ-secretase inhibitor DAPT 3 hours before DNFB challenge (blocking Notch signaling in all cell types) inhibited ear swelling at 12 hours and that the effect of DAPT became even more pronounced 24 hours after challenge (Figure 4A).

To understand the relative contribution of endothelial Notch signaling to inflammation, we asked to what extent endothelial cell-targeted loss and gain of Notch function would affect the contact hypersensitivity response. We found that mice with deletion of *Rbpj* in endothelial cells ($Rbpj^{i\Delta EC}$) showed a significant reduction in ear swelling 24 hours after challenge (Figure 4B). Complementary, mice that expressed constitutively active endothelial Notch1 ($NICD^{iEC\text{-}OE}$) responded by a significantly stronger ear swelling compared to controls (Figure 4C). Collectively, these results show that not only global but also endothelial Notch signaling modulates the contact hypersensitivity response.

Endothelial Notch signaling supports leukocyte recruitment

We next asked if Notch signaling also affected leukocyte recruitment to the inflamed lesion. By immunostaining and quantifying CD45+ cells in DNFB-treated ears 24 hours after challenge, we observed increased numbers of total leukocytes (Figure 4D and Figure IIIB in the online-only Data Supplement), CD3+ dermal T cells (Figure 4E and Figure IIIC in the online-only Data Supplement), and neutrophils (Ly6G+ cells, Figure 4F) in $NICD^{iEC\text{-}OE}$ mice when compared to control mice. $NICD^{iEC\text{-}OE}$ mice also showed increased recruitment of monocytes (CD11b+Ly6C+ cells, fraction of total CD45+ population, Figure 4G). These findings demonstrate that an amplification of endothelial Notch1 signaling promotes leukocyte recruitment to the inflamed dermis in murine contact hypersensitivity.

Notch regulates common inflammatory genes in human and mouse endothelial cells

To identify genes that were consistently altered by Notch signaling in activated endothelial cells, we next compared transcriptome data from mouse endothelial cells isolated from DNFB-treated ears of $NICD^{iEC\text{-}OE}$ mutants and HUVECs treated with siRNA targeting *JAG1* or *NOTCH1* and stimulated with IL-1β. This approach identified 11 genes that were differentially regulated by all conditions (Figure 4H), including *VCAM1* and *CX3CL1* as well as Notch target genes with established roles in vascular differentiation (*HEY1*, *EFNB2*).

Confirming our transcriptional data, immunostaining of sections from mouse ears with an antibody recognizing VCAM1 showed increased VCAM1 signal in $NICD^{iEC\text{-}OE}$ mice compared to controls (Figure 4I and Figure IIID in the online-only Data Supplement). VCAM1 is upregulated by DNFB exposure[45][25] and allows firm adhesion of T cells, monocytes, and eosinophils that express the integrin heterodimer α4β1/VLA-4. A neutralizing antibody to VLA-4 is furthermore reported to partially block DNFB-induced contact dermatitis[46][26], suggesting that the observed increase in VCAM1 is likely to be physiologically significant.

In conclusion, the NOTCH1 effect observed in cultured human endothelial cells translates at least in part to the *in vivo* situation and contributes to explain the phenotype of $NICD^{iEC\text{-}OE}$ mice in DNFB-induced contact hypersensitivity.

Inhibition of NOTCH1 does not affect NF-κB and AP-1 signal transduction in endothelial cells

To dissect the mechanism by which NOTCH1 supported endothelial inflammatory activation, we next assessed if NOTCH1 inhibition altered IL-1β-induced signaling in endothelial cells. The IL-1β-induced signaling cascade involves IKK- and MAPK-dependent activation of the master inflammatory transcription factors NF-κB (RELA and p50) and AP-1 (cJUN and cFOS)[47][27] and NOTCH1 has been reported to directly[3,4,11][3,4,11] or indirectly[48][28] promote the activity of the IKK signalosome complex. We found, however, no evidence for such crosstalk in IL-1β-stimulated HUVECs since *NOTCH1* knockdown by siRNA altered neither the phosphorylation, degradation or resynthesis of IκBα (Figure IVA in the online-only Data Supplement), nor the levels of DNA-binding NF-κB subunits RELA and p50 in nuclear lysates (Figure VC in the online-only Data Supplement). Furthermore, assessing AP-1 activation in IL-1β-stimulated HUVECs, we detected no change in the DNA-binding potential of active cJUN (cJUN pSer73) upon *NOTCH1* knockdown (Figure IVD in the online-only Data Supplement), and levels of cJUN phosphorylation remained unaltered (Figure IVE in the online-only Data Supplement). Levels of DNA-binding cFOS in nuclear lysates were undetectable (data not shown). Taken together, these data show that inhibition of NOTCH1 does not markedly alter the signal transduction cascades of NF-κB and AP-1 in HUVECs.

Genomic sites occupied by the NOTCH1 transcription complex are also binding sites for RELA

Considering that NOTCH1 inhibition markedly reduced the upregulation of selected inflammatory genes but had little impact on inflammatory signaling cascades, we asked if the NOTCH1 transcription complex might in itself promote favorable conditions for transcriptional activation of these genes. We therefore profiled the genome-wide binding of canonical components of the NOTCH1 transcription complex (NOTCH1-RBPJ) and the NF-κB subunit RELA, as well as the deposition of histone H3 acetylated at lysine 27 (H3K27ac), a measure of enhancer activity[49][29] that can be promoted by the genomic impact of both NOTCH1[17,18][17,18] and NF-κB[16,50][16,30]. Chromatin immunoprecipitation combined with deep sequencing (ChIP-seq) was first performed in confluent, resting HUVECs to generate genome-wide binding profiles of NOTCH1 and RBPJ, identifying a total of 4,328 and 11,345 peaks (Figure VA in the online-only Data Supplement). Strikingly, when profiling the binding of RELA by ChIP-seq in IL-1β-stimulated HUVECs, we discovered that the vast majority of DNA binding sites for NOTCH1 and RBPJ in unstimulated cells overlapped with sites bound by RELA in IL-1β-stimulated cells (97% and 83% basepair overlap; Figure 5A). Moreover, global RELA binding was not reduced by knockdown of *NOTCH1* (Figures VA and VB in the online-only Data Supplement), supporting the notion that NOTCH1 is dispensable for RELA signal transduction and its genomic binding in endothelial cells.

The NOTCH1 transcription complex promotes activation of inflammatory enhancers

We next manually explored the binding of the NOTCH1 transcription complex in the proximity to JAG1/NOTCH1-supported genes. RBPJ peaks were identified in or close to transcriptional start sites of canonical NOTCH1 target genes including *HES1* (Figure 5B) and *IL33* (Figure VIA in the online-only Data Supplement), as well as some of the JAG1/NOTCH1-supported genes involved in leukocyte recruitment, including *ICAM1* (Figure 5C) and *SELP* (Figure VIB in the online-only Data Supplement). In contrast, RBPJ did not bind in or near transcriptional start sites of the JAG1/NOTCH1-supported genes *VCAM1* (Figure 5D), *CCL7*, or *CCL8* (Figure 5E), but instead occupied nearby (+/- 100kB) regions recently described as "inflammatory super-enhancers", based on strong, TNF-α-induced BRD4 enrichment[16][16]. Interestingly, the RBPJ-peak close to the *ICAM1* transcriptional start site was also associated with one of these inflammatory enhancers (Figure 5C). In all examined regions, NOTCH1 binding patterns mirrored those of RBPJ, but the signal was generally weaker, resulting in fewer called peaks.

Notably, the identified NOTCH1/RBPJ peaks in the *VCAM1*-assigned enhancer overlapped with binding of RELA in IL-1β-stimulated cells (Figure 6A), and NOTCH1 knockdown almost

completely abrogated the IL-1β-induced activity around this site as judged by the deposition of H3K27ac (Figure 6A). The same pattern was observed in the inflammatory enhancer region associated with the *CCL2-CCL7-CCL11-CCL8* locus (Figure 6B).

Our findings prompted us to ask whether the NOTCH1 transcription complex exerted a net effect on the activation of inflammatory enhancers. Taking advantage of the previously defined set of inflammatory enhancers[16,16], we detected RELA binding within all of these regions and found that a large subset was also bound by NOTCH1 (41%) and/or RBPJ (77%) (Figure 6C). Importantly, when focusing on those regions containing NOTCH1 peaks (all of which also contained RBPJ peaks, Figure 6C), we discovered that the increased mean peak intensity of H3K27ac elicited by IL-1β stimulation was strongly attenuated upon *NOTCH1* knockdown (Figure 6D). Furthermore, the extent of H3K27ac peak overlap within the same regions was reduced by 31% following *NOTCH1* knockdown (Figure 6E). Taken together, these results suggest that the transcription complex of NOTCH1-RBPJ facilitates activation of a subset of strong NF-κB-directed enhancers central to the endothelial inflammatory response that mediates leukocyte recruitment.

Discussion

Endothelial cell activation is a crucial component of the inflammatory response. Here, we provide the first evidence that NOTCH1 supports the inflammatory endothelial phenotype that mediates leukocyte recruitment by facilitating activation of inflammation-driven enhancers. Our conclusions build on the following observations: First, we demonstrate that JAG1/NOTCH1 globally modulates the transcriptional response to inflammatory cytokines. Second, we observe that NOTCH1 signaling contributes to the inflammatory response *in vivo*, and, third, we show that the transcription complex acting downstream of NOTCH1 signaling occupies inflammatory loci targeted by NF-κB and facilitates activation of inflammatory enhancers central to the endothelial inflammatory program[16,16].

Previous data demonstrate that NOTCH1 signaling may promote inflammatory activation by crosstalk with inflammatory signaling cascades, perhaps best illustrated in the NF-κB pathway. For example, NOTCH1 can induce NF-κB activation and cellular survival in cancer cells by direct interactions between NICD1 and the IKK signalosome that facilitates cytoplasmic IκBα degradation[3,4,3,4]. NICD1 has also been reported to directly interact with NF-κB subunits, affecting their nuclear import and retention[11,51,52,11,31,32]. It nevertheless appears, based on our analyses, that these mechanisms are of less importance in human endothelial cells. Our combined findings demonstrate that acute NF-κB signaling to RELA-p50 remains unaffected by *NOTCH1* knockdown and that the recruitment of RELA to chromatin, as assessed by genome-wide ChIP-sequencing, is not reduced. This agrees with observations made by ourselves and others[10,10] that some NF-κB targets, like CXCL8 and CXCL1, remain unaffected or are even induced by NOTCH1 inhibition. Moreover, the current model cannot explain how NOTCH1 supports the expression of P-selectin, another leukocyte-recruiting molecule that is not driven by NF-κB activation.

By contrast, our data indicate that NOTCH1 supports inflammatory activation of endothelial cells at the chromatin level by globally promoting inflammatory enhancer activity, and that its transcription complex also binds directly to the transcriptional start sites of some inflammatory genes (*SELP, ICAM1*). Indeed, we discovered that most sites occupied by the NOTCH1 transcription complex in endothelial cells are inflammatory in the sense that they are bound by RELA after IL-1β-stimulation. Although our data are the first to reveal an effect of NOTCH1 on inflammatory enhancers, NOTCH1 has been reported to promote recruitment of IKKα to IKKα-stimulated promoters in cervical cancer cells[4,4], indicating that it may also support the ability of IKKα to mediate derepression of NF-κB target genes[5,33,3,3]. Altogether, our data takes the understanding of NOTCH1 function in inflammation to a new level by demonstrating a profound involvement in inflammatory enhancer activation.

Our data support a model in which the NOTCH1 transcription complex assists the NF-κB-driven machinery in orchestrating activation of inflammatory enhancers central to controlling the endothelial inflammatory phenotype. Notably, this mode of regulation was apparent at the *VCAM1* locus (Figures 5D and 6A), which stood out as one of the most robustly NOTCH1-supported genes in our transcriptional analyses. It should be noted that while the depicted enhancer was recently assigned to *VCAM1*[16], its functional impact on *VCAM1* expression remains to be confirmed, *e.g.* by genomic deletion or epigenetic inactivation of the enhancer. Of note, the enhancer is directly associated with a long intergenic nonprotein-coding RNA (LINCO1349) and NOTCH1 has previously been shown to coregulate coding transcripts without an obvious NOTCH1 binding site near the transcriptional start site and noncoding transcripts associated with distal NOTCH1-bound enhancers[54]. Another interesting enhancer region is associated with the *CCL2-CCL7-CCL11-CCL8* locus (Figures 5E and 6B). We observed that while basal *CCL2* expression was consistently supported by NOTCH1 in unstimulated HUVECs, neither JAG1 nor NOTCH1 inhibition had any effect on its upregulation after IL-1β-stimulation (Figure 1C, Table I in the online-only Data Supplement, and submitted microarray data GSE85987). In contrast, JAG1 and NOTCH1 supported the IL-1β-stimulated transcriptional upregulation of the adjacent genes *CCL7* and *CCL8* (Figure 1C, Table I in the online-only Data Supplement, and submitted microarray data GSE85987), perhaps by facilitating the activation of the enhancer region associated with the *CCL2* transcriptional start site (Figures 5E and 6B). Because many enhancers regulate cognate genes over considerable distances[55], target gene(s) of a given enhancer cannot be accurately predicted simply by genomic distance. So far, no studies have reported chromosome conformation data from inflammatory activated HUVECs, making it difficult to make valid predictions of chromatin folding. To promote a better understanding of how NOTCH1 controls the expression of inflammatory genes in HUVECs, it is therefore crucial that future experimental approaches are designed to map the three-dimensional chromatin structure in relation to RBPJ-NOTCH1 binding sites in the context of inflammatory activation.

Emerging evidence adds support to the notion that cell fate-regulating transcription factors other than the NOTCH1 transcription complex also modulate chromatin at inflammatory enhancers. Illustrating this, lineage-specific expression of stress-inducible target genes of NF-κB, AP-1, and IRF1 in monocytes/macrophages are programmed by the cell fate-regulating transcription factor PU.1 in synergy with C/EBPα[56,57]. In a complementary manner, our findings demonstrate that the Notch signaling system dynamically modulates the responsiveness of endothelial cells to proinflammatory cytokine activation.

A fascinating aspect of Notch signaling is the relative contribution of individual Notch ligands to receptor activation. Ligand-specific biological outcomes appear to depend on differences in signal strength and have been demonstrated in inner ear development[58], T cell differentiation[59], and during angiogenesis where endothelial JAG1 acts as a competitive antagonist to DLL4[20]. The selective responsiveness of JAG1 to proinflammatory endothelial activation motivated our initial transcriptional screen of the response to *JAG1* knockdown, showing a profound effect of JAG1 on endothelial activation. However, subsequent, unpublished experiments in mice with endothelial cell-specific deletion of *Jag1* failed to show significant effects on inflammation in the DNFB-induced contact hypersensitivity model (Edelmann *et al.*, unpublished). In contrast, endothelial loss of the canonical Notch transcription factor *Rbpj* markedly reduced inflammation, suggesting that signaling by other endothelial Notch ligands or ligands expressed by cell types other than endothelial cells promoted inflammatory activation in this model. Supporting the concept that several Notch ligands can drive the proinflammatory effect of NOTCH1, we found that knockdown of either *JAG1* or *DLL4* in confluent endothelial cell cultures inhibited VCAM1 expression in a similar manner, despite the dramatic increase in JAG1 levels during the time period investigated. Notably, we did not observe any evidence of increased NOTCH1 activity in IL-1β-stimulated cells, despite the upregulation of JAG1 expression. It is therefore tempting to speculate that the upregulation of JAG1 by proinflammatory cytokines at least partly serves to compensate

for the downregulation of other more potent Notch ligands, like DLL4. Moreover, the ability of individual Notch ligands to induce or inhibit signaling will vary according to the presence of other Notch ligands[5838], the *cis*- and *trans*-expression of Notch receptors[6040], and the glycosylation status of these receptors[2020]. The functional impact of JAG1 induction in a physiological setting therefore remains unsettled, but invites further investigation.

Although this study was focused on understanding the role of NOTCH1 signaling in endothelial cell activation, assessment of global Notch inhibition as a treatment modality in inflammatory disease may be of even greater therapeutic interest. To this end, the currently most impressive demonstration of Notch involvement in an inflammatory context is perhaps the observation that inhibition of selected Notch ligands control murine graft-versus-host-disease with no overt side effects[88]. We therefore propose that the relative contribution of individual Notch components to different inflammatory processes is highly deserving of future exploration. To this end, it will be interesting to systematically assess how Notch ligands and receptors contribute to chronic inflammatory diseases and to what extent components of the Notch pathway are suitable for therapeutic targeting.

Accession numbers

Microarray and ChIP-seq data are accessible through GEO accession number GSE85987.

Acknowledgements

We thank Martin Stehling (Flow Cytometry Unit, Max-Planck Institute for Molecular Biomedicine, Münster) for assisting with endothelial cell sorting; Aaste Aursjø*, Sara Halmøy Bakke, Kathrine Hagelsteen, Filip Nikolaysen, Hogne Røed Nilsen, Danh Phung, Linda Solfjell, Frank Sætre, and Kjersti Thorvaldsen Hagen (Laboratory for Immunohistochemistry and Immunopathology, Department of Pathology, Oslo University Hospital (OUH)) for excellent technical assistance; staff at the Norwegian Microarray Consortium (NMC) and Genomics Core Facility, Oslo University Hospital (OUH) for assisting with microarray and sequencing experiments; and staff at the Department of Gynecology and Obstetrics, OUH, for assistance with collecting umbilical cords.

*deceased

Sources of funding

Funding was obtained from The South-Eastern Norway Regional Health Authorities (2010051, 2010019, 2013115, 2014032, 2017061), the Norwegian Cancer Society (20060448, 20070199, 201233376), the Research Council of Norway (221929/F20), and the University of Oslo (131406).

Disclosures

Christian W. Siebel is employed by Genentech Inc.

References

1. Hori K, Sen A, Artavanis-Tsakonas S. Notch signaling at a glance. *Journal of Cell Science*. 2013;126(Pt 10):2135–2140.

2. Schwanbeck R, Martini S, Bernoth K, Just U. The Notch signaling pathway: molecular basis of cell context dependency. *European Journal of Cell Biology*. 2011;90(6-7):572–581.

3. Vilimas T, Mascarenhas J, Palomero T, Mandal M, Buonamici S, Meng F, Thompson B, Spaulding C, Macaroun S, Alegre M-L, Kee BL, Ferrando A, Miele L, Aifantis I. Targeting the NF-κB signaling pathway in Notch1-induced T-cell

leukemia. *Nat Med*. 2006;13(1):70–77.

4. Song LL, Peng Y, Yun J, et al. Notch-1 associates with IKKα and regulates IKK activity in cervical cancer cells. *Oncogene*. 2008;27(44):5833–5844.

5. Park J-S, Kim S-H, Kim K, et al. Inhibition of Notch signalling ameliorates experimental inflammatory arthritis. *Ann Rheum Dis*. November 2013.

6. Aziz M, Ishihara S, Ansary MU, et al. Crosstalk between TLR5 and Notch1 signaling in epithelial cells during intestinal inflammation. *Int J Mol Med*. 2013;32(5):1051–1062.

7. Han H, Gong G, Bai X, Lin Y-C, Sun J, Wang W, Zhao Y, Yang L, Wang X, Zhang Z, Dong H, Hou L, Xiong L. Inhibition of notch signaling protects mouse lung against zymosan-induced injury. *Shock*. 2013;40(4):312–319.

8. Tran IT, Sandy AR, Carulli AJ, et al. Blockade of individual Notch ligands and receptors controls graft-versus-host disease. *J Clin Invest*. 2013;123(4):1590–1604.

9. Vestweber D. How leukocytes cross the vascular endothelium. *Nat Rev Immunol*. 2015;15(11):692–704.

10. Briot A, Civelek M, Seki A, et al. Endothelial NOTCH1 is suppressed by circulating lipids and antagonizes inflammation during atherosclerosis. *J Exp Med*. 2015;212(12):2147–2163.

11. Nus M, Martínez-Poveda B, Macgrogan D, Chevre R, D'Amato G, Sbroggio M, Rodríguez C, Martínez-González J, Andrés V, Hidalgo A, la Pompa de JL. Endothelial Jag1-RBPJ signalling promotes inflammatory leukocyte recruitment and atherosclerosis. *Cardiovasc Res*. August 2016:cvw193.

12. Verginelli F, Adesso L, Limon I, et al. Activation of an endothelial Notch1-Jagged1 circuit induces VCAM1 expression, an effect amplified by interleukin-1β. *Oncotarget*. 2015;6(41):43216–43229.

13. Wieland E, Rodriguez-Vita J, Liebler SS, et al. Endothelial Notch1 Activity Facilitates Metastasis. *Cancer Cell*. February 2017.

14. Quillard T, Coupel S, Coulon F, Fitau J, Chatelais M, Cuturi MC, Chiffoleau E, Charreau B. Impaired Notch4 Activity Elicits Endothelial Cell Activation and Apoptosis: Implication for Transplant Arteriosclerosis. *Arterioscler Thromb Vasc Biol*. 2008;28(12):2258–2265.

15. Kempe S. NF-kB controls the global pro-inflammatory response in endothelial cells: evidence for the regulation of a pro-atherogenic program. *Nucleic Acids Res*. 2005;33(16):5308–5319.

16. Brown JD, Lin CY, Duan Q, et al. NF-kB Directs Dynamic Super Enhancer Formation in Inflammation and Atherogenesis. *Mol Cell*. 2014;56(2):219–231.

17. Wang H, Zang C, Taing L, Arnett KL, Wong YJ, Pear WS, Blacklow SC, Liu XS, Aster JC. NOTCH1-RBPJ complexes drive target gene expression through dynamic interactions with superenhancers. *Proc Natl Acad Sci U S A*. 2014;111(2):705–710.

18. Castel D, Mourikis P, Bartels SJJ, Brinkman AB, Tajbakhsh S, Stunnenberg HG. Dynamic binding of RBPJ is determined by Notch signaling status. *Genes Dev*. 2013;27(9):1059–1071.

19. Jaffe EA, Nachman RL, Becker CG, Minick CR. Culture of Human Endothelial Cells Derived from Umbilical Veins. Identification by morphologic and immunologic criteria. *J Clin Invest*. 1973;52(11):2745–2756.

20. Benedito R, Roca C, Sörensen I, Adams S, Gossler A, Fruttiger M, Adams RH. The Notch Ligands Dll4 and Jagged1 Have Opposing Effects on Angiogenesis. *Cell*. 2009;137(6):1124–1135.

21. Hummon AB, Lim SR, Difilippantonio MJ, Ried T. Isolation and solubilization of proteins after TRIzol extraction of RNA and DNA from patient material following prolonged storage. *BioTechniques*. 2007;42(4):467–70–472.

22. Haraldsen G, Sollid LM, Bakke O, Farstad IN, Kvale D, Molberg, Norstein J, Stang E, Brandtzaeg P. Major histocompatibility complex class II-dependent antigen presentation by human intestinal endothelial cells. *Gastroenterology*. 1998;114(4):649–656.

23. Ron Edgar MDAEL. Gene Expression Omnibus: NCBI gene expression and hybridization array data repository. *Nucleic Acids Res*. 2002;30(1):207.

24. Dunning MJ, Smith ML, Ritchie ME, Tavaré S. beadarray: R classes and methods for Illumina bead-based data. *Bioinformatics*. 2007;23(16):2183–2184.

25. Carvalho BS, Irizarry RA. A framework for oligonucleotide microarray preprocessing. *Bioinformatics*. 2010.

26. Ritchie ME, Phipson B, Di Wu, Hu Y, Law CW, Shi W, Smyth GK. Limma powers differential expression analyses for RNA-sequencing and microarray studies. *Nucleic Acids Res*. 2015;43(7):e47–e47.

27. Ashburner M, Ball CA, Blake JA, et al. Gene Ontology: tool for the unification of biology. *Nat Genet*. 2000;25(1):25–29.

28. Schmittgen TD, Livak KJ. Analyzing real-time PCR data by the comparative C(T) method. *Nat Protoc*. 2008;3(6):1101–1108.

29. Küchler AM, Pollheimer J, Balogh J, Sponheim J, Manley L, Sorensen DR, De Angelis PM, Scott H, haraldsen G. Nuclear Interleukin-33 Is Generally Expressed in Resting Endothelium but Rapidly Lost upon Angiogenic or Proinflammatory Activation. *Am J Pathol*. 2008;173(4):1229–1242.

30. Nowak DE, Tian B, Brasier AR. Two-step cross-linking method for identification of NF-kappaB gene network by chromatin immunoprecipitation. *BioTechniques*. 2005;39(5):715–725.

31. Langmead B, Salzberg SL. Fast gapped-read alignment with Bowtie 2. *Nat Meth*. 2012;9(4):357–359.

32. Li H, Handsaker B, Wysoker A, Fennell T, Ruan J, Homer N, Marth G, Abecasis G, Durbin R, 1000 Genome Project Data Processing Subgroup. The Sequence Alignment/Map format and SAMtools. *Bioinformatics*. 2009;25(16):2078–2079.

33. Thorvaldsdóttir H, Robinson JT, Mesirov JP. Integrative Genomics Viewer (IGV): high-performance genomics data visualization and exploration. *Brief Bioinformatics*. 2013;14(2):178–192.

34. Zhang Y, Liu T, Meyer CA, Eeckhoute J, Johnson DS, Bernstein BE, Nusbaum C, Myers RM, Brown M, Li W, Liu XS. Model-based Analysis of ChIP-Seq (MACS). *Genome Biol*. 2008;9(9):R137.

35. Quinlan AR, Hall IM. BEDTools: a flexible suite of utilities for comparing genomic features. *Bioinformatics*. 2010;26(6):841–842.

36. Shen L, Shao N, Liu X, Nestler E. ngs.plot: Quick mining and visualization of next-generation sequencing data by integrating genomic databases. *BMC Genomics*. 2014;15(1):284.

37. RCoreTeam. R: A Language and Environment for Statistical Computing. cran.r-project.org. https://cran.r-project.org/doc/manuals/r-release/fullrefman.pdf. Published September 23, 2016. Accessed September 23, 2016.

38. Wickham H. *Ggplot2*. New York, NY: Springer New York; 2009.

39. Pitulescu ME, Schmidt I, Benedito R, Adams RH. Inducible gene targeting in the neonatal vasculature and analysis of retinal angiogenesis in mice. *Nat Protoc*. 2010;5(9):1518–1534.

40. Johnston DA, Dong B, Hughes CCW. TNF induction of jagged-1 in endothelial cells is NFκB-dependent. *Gene*. 2009;435(1-2):36–44.

41. Sainson RCA, Johnston DA, Chu HC, Holderfield MT, Nakatsu MN, Crampton SP, Davis J, Conn E, Hughes CCW. TNF primes endothelial cells for angiogenic sprouting by inducing a tip cell phenotype. *Blood*. 2008;111(10):4997–5007. doi:10.1182/blood-2007-08-108597.

42. Brütsch R, Liebler SS, Wüstehube J, Bartol A, Herberich SE, Adam MG, Telzerow A, Augustin HG, Fischer A. Integrin cytoplasmic domain-associated protein-1 attenuates sprouting angiogenesis. *Circulation Research*. 2010;107(5):592–601.

43. Kluk MJ, Ashworth T, Wang H, et al. Gauging NOTCH1 Activation in Cancer Using Immunohistochemistry. Martinez Climent JA, ed. *PLoS ONE*. 2013;8(6):e67306.

44. Middleton J, Americh L, Gayon R, Julien D, Mansat M, Mansat P, Anract P, Cantagrel A, Cattan P, Reimund J-M, Aguilar L, Amalric F, Girard J-P. A comparative study of endothelial cell markers expressed in chronically inflamed human tissues: MECA-79, Duffy antigen receptor for chemokines, von Willebrand factor, CD31, CD34, CD105 and CD146. *J Pathol*. 2005;206(3):260–268.

45. Henseleit U, Steinbrink K, Sunderkötter C, Goebeler M, Roth J, Sorg C. Expression of murine VCAM-1 in vitro and in different models of inflammation in vivo: correlation with immigration of monocytes. *Exp Dermatol*. 1995;4(5):249–256.

46. Takeshita K, Yamasaki T, Akira S, Gantner F, Bacon KB. Essential role of MHC

II-independent CD4+ T cells, IL-4 and STAT6 in contact hypersensitivity induced by fluorescein isothiocyanate in the mouse. *International Immunology*. 2004;16(5):685–695.

47. Pober JS, Sessa WC. Evolving functions of endothelial cells in inflammation. *Nat Rev Immunol*. 2007;7(10):803–815. doi:10.1038/nri2171.

48. Espinosa L, Cathelin S, D'Altri T, et al. The Notch/Hes1 Pathway Sustains NF-κB Activation through CYLD Repression in T Cell Leukemia. *Cancer Cell*. 2010;18(3):268–281.

49. Creyghton MP, Cheng AW, Welstead GG, Kooistra T, Carey BW, Steine EJ, Hanna J, Lodato MA, Frampton GM, Sharp PA, Boyer LA, Young RA, Jaenisch R. Histone H3K27ac separates active from poised enhancers and predicts developmental state. *Proc Natl Acad Sci USA*. 2010;107(50):21931–21936.

50. Zhong H, May MJ, Jimi E, Ghosh S. The phosphorylation status of nuclear NF-kappa B determines its association with CBP/p300 or HDAC-1. *Mol Cell*. 2002;9(3):625–636.

51. Wang J, Shelly L, Miele L, Boykins R, Norcross MA, Guan E. Human Notch-1 inhibits NF-kappa B activity in the nucleus through a direct interaction involving a novel domain. *J Immunol*. 2001;167(1):289–295.

52. Shin HM, Minter LM, Cho OH, Gottipati S, Fauq AH, Golde TE, Sonenshein GE, Osborne BA. Notch1 augments NF-κB activity by facilitating its nuclear retention. *EMBO J*. 2005;25(1):129–138.

53. Hoberg JE, Yeung F, Mayo MW. SMRT derepression by the IkappaB kinase alpha: a prerequisite to NF-kappaB transcription and survival. *Mol Cell*. 2004;16(2):245–255.

54. Severson E, Arnett KL, Wang H, Zang C, Taing L, Liu H, Pear WS, Liu XS, Blacklow SC, Aster JC. Genome-wide identification and characterization of Notch transcription complex-binding sequence-paired sites in leukemia cells. *Sci Signal*. 2017;10(477).

55. Amano T, Sagai T, Tanabe H, Mizushina Y, Nakazawa H, Shiroishi T. Chromosomal Dynamics at theShhLocus: Limb Bud-Specific Differential Regulation of Competence and Active Transcription. *Dev Cell*. 2009;16(1):47–57.

56. Ghisletti S, Barozzi I, Mietton F, Polletti S, De Santa F, Venturini E, Gregory L, Lonie L, Chew A, Wei C-L, Ragoussis J, Natoli G. Identification and characterization of enhancers controlling the inflammatory gene expression program in macrophages. *Immunity*. 2010;32(3):317–328.

57. Jin F, Li Y, Ren B, Natarajan R. PU.1 and C/EBP synergistically program distinct response to NF- B activation through establishing monocyte specific enhancers. *Proc Natl Acad Sci U S A*. 2011;108(13):5290–5295.

58. Petrovic J, Formosa-Jordan P, Luna-Escalante JC, Abelló G, Ibañes M, Neves J, Giraldez F. Ligand-dependent Notch signaling strength orchestrates lateral induction and lateral inhibition in the developing inner ear. *Development*. 2014;141(11):2313–2324.

59. Van de Walle I, Waegemans E, De Medts J, et al. Specific Notch receptor-ligand interactions control human TCR-αβ/γδ development by inducing differential Notch signal strength. *J Exp Med*. 2013;210(4):683–697.

60. Sprinzak D, Lakhanpal A, LeBon L, Santat LA, Fontes ME, Anderson GA, Garcia-Ojalvo J, Elowitz MB. Cis-interactions between Notch and Delta generate mutually exclusive signalling states. *Nature*. 2010;465(7294):86–90.

1. Hori K, Sen A, Artavanis-Tsakonas S. Notch signaling at a glance. *Journal of Cell Science*. 2013;126:2135–2140.

2. Schwanbeck R, Martini S, Bernoth K, Just U. The Notch signaling pathway: molecular basis of cell context dependency. *European Journal of Cell Biology*. 2011;90:572–581.

3. Vilimas T, Mascarenhas J, Palomero T, Mandal M, Buonamici S, Meng F, Thompson B, Spaulding C, Macaroun S, Alegre M-L, Kee BL, Ferrando A, Miele L, Aifantis I. Targeting the NF-κB signaling pathway in Notch1-induced T-cell leukemia. *Nat Med*. 2006;13:70–77.

4. Song LL, Peng Y, Yun J, et al. Notch-1 associates with IKKα and regulates IKK activity in cervical cancer cells. *Oncogene*. 2008;27:5833–5844.

5. Park J-S, Kim S-H, Kim K, et al. Inhibition of Notch signalling ameliorates experimental inflammatory arthritis. *Ann Rheum Dis*. 2015 Jan;74:267–74.

6. Aziz M, Ishihara S, Ansary MU, et al. Crosstalk between TLR5 and Notch1 signaling in epithelial cells during intestinal inflammation. *Int J Mol Med*. 2013;32:1051–1062.

7. Han H, Gong G, Bai X, Lin Y-C, Sun J, Wang W, Zhao Y, Yang L, Wang X, Zhang Z, Dong H, Hou L, Xiong L. Inhibition of notch signaling protects mouse lung against zymosan-induced injury. *Shock*. 2013;40:312–319.

8. Tran IT, Sandy AR, Carulli AJ, et al. Blockade of individual Notch ligands and receptors controls graft-versus-host disease. *J Clin Invest*. 2013;123:1590–1604.

9. Vestweber D. How leukocytes cross the vascular endothelium. *Nat Rev Immunol*. 2015;15:692–704.

10. Briot A, Civelek M, Seki A, et al. Endothelial NOTCH1 is suppressed by circulating lipids and antagonizes inflammation during atherosclerosis. *J Exp Med*. 2015;212:2147–2163.

11. Nus M, Martínez-Poveda B, Macgrogan D, Chevre R, D'Amato G, Sbroggio M, Rodríguez C, Martínez-González J, Andrés V, Hidalgo A, la Pompa de JL. Endothelial Jag1-RBPJ signalling promotes inflammatory leukocyte recruitment and atherosclerosis. *Cardiovasc Res*. August 2016:cvw193 [Epub ahead of print].

12. Verginelli F, Adesso L, Limon I, et al. Activation of an endothelial Notch1-Jagged1 circuit induces VCAM1 expression, an effect amplified by interleukin-1β. *Oncotarget*. 2015;6:43216–43229.

13. Wieland E, Rodriguez-Vita J, Liebler SS, et al. Endothelial Notch1 Activity

Facilitates Metastasis. *Cancer Cell*. 2017; Mar 13;31:355-367.

14. Quillard T, Coupel S, Coulon F, Fitau J, Chatelais M, Cuturi MC, Chiffoleau E, Charreau B. Impaired Notch4 Activity Elicits Endothelial Cell Activation and Apoptosis: Implication for Transplant Arteriosclerosis. *Arterioscler Thromb Vasc Biol*. 2008;28:2258–2265.

15. Kempe S, NF-κB controls the global pro-inflammatory response in endothelial cells: evidence for the regulation of a pro-atherogenic program. *Nucleic Acids Res*. 2005;33:5308–5319.

16. Brown JD, Lin CY, Duan Q, et al. NF-kB Directs Dynamic Super Enhancer Formation in Inflammation and Atherogenesis. *Mol Cell*. 2014;56:219–231.

17. Wang H, Zang C, Taing L, Arnett KL, Wong YJ, Pear WS, Blacklow SC, Liu XS, Aster JC. NOTCH1-RBPJ complexes drive target gene expression through dynamic interactions with superenhancers. *Proc Natl Acad Sci U S A*. 2014;111:705–710.

18. Castel D, Mourikis P, Bartels SJJ, Brinkman AB, Tajbakhsh S, Stunnenberg HG. Dynamic binding of RBPJ is determined by Notch signaling status. *Genes Dev*. 2013;27:1059–1071.

19. Johnston DA, Dong B, Hughes CCW. TNF induction of jagged-1 in endothelial cells is NFκB-dependent. *Gene*. 2009;435:36–44.

20. Benedito R, Roca C, Sörensen I, Adams S, Gossler A, Fruttiger M, Adams RH. The Notch Ligands Dll4 and Jagged1 Have Opposing Effects on Angiogenesis. *Cell*. 2009;137:1124–1135.

21. Sainson RCA, Johnston DA, Chu HC, Holderfield MT, Nakatsu MN, Crampton SP, Davis J, Conn E, Hughes CCW. TNF primes endothelial cells for angiogenic sprouting by inducing a tip cell phenotype. *Blood*. 2008;111:4997–5007.

22. Brütsch R, Liebler SS, Wüstehube J, Bartol A, Herberich SE, Adam MG, Telzerow A, Augustin HG, Fischer A. Integrin cytoplasmic domain-associated protein-1 attenuates sprouting angiogenesis. *Circulation Research*. 2010;107:592–601.

23. Kluk MJ, Ashworth T, Wang H, et al. Gauging NOTCH1 Activation in Cancer Using Immunohistochemistry. *PLoS ONE*. 2013; 2013 Jun 18;8(6):e67306.

24. Middleton J, Americh L, Gayon R, Julien D, Mansat M, Mansat P, Anract P, Cantagrel A, Cattan P, Reimund J-M, Aguilar L, Amalric F, Girard J-P. A comparative study of endothelial cell markers expressed in chronically inflamed human tissues: MECA-79, Duffy antigen receptor for chemokines, von Willebrand factor, CD31, CD34, CD105 and CD146. *J Pathol*. 2005;206:260–268.

25. Henseleit U, Steinbrink K, Sunderkötter C, Goebeler M, Roth J, Sorg C. Expression of murine VCAM-1 in vitro and in different models of inflammation in vivo: correlation with immigration of monocytes. *Exp Dermatol*. 1995;4:249–256.

26. Takeshita K, Yamasaki T, Akira S, Gantner F, Bacon KB. Essential role of MHC II-independent CD4+ T cells, IL-4 and STAT6 in contact hypersensitivity induced

by fluorescein isothiocyanate in the mouse. *International Immunology*. 2004;16:685–695.

27. Pober JS, Sessa WC. Evolving functions of endothelial cells in inflammation. *Nat Rev Immunol*. 2007;7:803–815.

28. Espinosa L, Cathelin S, D'Altri T, et al. The Notch/Hes1 Pathway Sustains NF-κB Activation through CYLD Repression in T Cell Leukemia. *Cancer Cell*. 2010;18:268–281.

29. Creyghton MP, Cheng AW, Welstead GG, Kooistra T, Carey BW, Steine EJ, Hanna J, Lodato MA, Frampton GM, Sharp PA, Boyer LA, Young RA, Jaenisch R. Histone H3K27ac separates active from poised enhancers and predicts developmental state. *Proc Natl Acad Sci USA*. 2010;107:21931–21936.

30. Zhong H, May MJ, Jimi E, Ghosh S. The phosphorylation status of nuclear NF-kappa B determines its association with CBP/p300 or HDAC-1. *Mol Cell*. 2002;9:625–636.

31. Wang J, Shelly L, Miele L, Boykins R, Norcross MA, Guan E. Human Notch-1 inhibits NF-kappa B activity in the nucleus through a direct interaction involving a novel domain. *J Immunol*. 2001;167:289–295.

32. Shin HM, Minter LM, Cho OH, Gottipati S, Fauq AH, Golde TE, Sonenshein GE, Osborne BA. Notch1 augments NF-κB activity by facilitating its nuclear retention. *EMBO J*. 2005;25:129–138.

33. Hoberg JE, Yeung F, Mayo MW. SMRT derepression by the IkappaB kinase alpha: a prerequisite to NF-kappaB transcription and survival. *Mol Cell*. 2004;16:245–255.

34. Severson E, Arnett KL, Wang H, Zang C, Taing L, Liu H, Pear WS, Liu XS, Blacklow SC, Aster JC. Genome-wide identification and characterization of Notch transcription complex-binding sequence-paired sites in leukemia cells. *Sci Signal*. 2017;10.

35. Amano T, Sagai T, Tanabe H, Mizushina Y, Nakazawa H, Shiroishi T. Chromosomal Dynamics at the Shh Locus: Limb Bud-Specific Differential Regulation of Competence and Active Transcription. *Dev Cell*. 2009;16:47–57.

36. Ghisletti S, Barozzi I, Mietton F, Polletti S, De Santa F, Venturini E, Gregory L, Lonie L, Chew A, Wei C-L, Ragoussis J, Natoli G. Identification and characterization of enhancers controlling the inflammatory gene expression program in macrophages. *Immunity*. 2010;32:317–328.

37. Jin F, Li Y, Ren B, Natarajan R. PU.1 and C/EBP synergistically program distinct response to NF-κB activation through establishing monocyte specific enhancers. *Proc Natl Acad Sci U S A*. 2011;108:5290–5295.

38. Petrovic J, Formosa-Jordan P, Luna-Escalante JC, Abelló G, Ibañes M, Neves J, Giraldez F. Ligand-dependent Notch signaling strength orchestrates lateral induction and lateral inhibition in the developing inner ear. *Development*. 2014;141:2313–2324.

39. Van de Walle I, Waegemans E, De Medts J, et al. Specific Notch receptor-ligand

interactions control human TCR-αβ/γδ development by inducing differential Notch signal strength. *J Exp Med*. 2013;210:683–697.

40. Sprinzak D, Lakhanpal A, LeBon L, Santat LA, Fontes ME, Anderson GA, Garcia-Ojalvo J, Elowitz MB. Cis-interactions between Notch and Delta generate mutually exclusive signalling states. *Nature*. 2010;465:86–90.

Highlights

- Conditional genetic targeting of endothelial Notch modulates inflammation in murine contact hypersensitivity.
- RBPJ-NOTCH1 premarks sites of RELA genomic recruitment in endothelial cells.
- Endothelial NOTCH1 facilitates the activation of inflammatory enhancers.

Formatted: Heading 2, Indent: Left: 0", First line: 0", Space After: 0 pt, Widow/Orphan control, Adjust space between Latin and Asian text, Adjust spa between Asian text and numbers, Tab stops: Not at 0.83"

Figure legends

Figure 1: *Endothelial JAG1 expression is upregulated by inflammatory stimuli and supports endothelial cell activation.* (**A**) HUVECs were treated with IL-1β (1 ng/ml), TNF-α (1 ng/ml) or IFN-γ (50 ng/ml) for 6 hours and analyzed by RT-qPCR. Bars show mean ± SD of 3 experiments in cells from different donors. *JAG1* expression was induced by IL-1β (p=0.0156), TNF-α (p=0. 0156), and IFN-γ (p=0. 0156), Wilcoxon signed rank test. (**B**-**C**) HUVECs (7 donor pool, n=3) were treated with siRNA (scrambled or *JAG1*, 40nM) and stimulated with IL-1β (5 ng/ml, 24h) before transcriptional profiling. (**B**) The bar chart shows the most specific terms enriched in the population of genes suppressed or induced by *JAG1* knockdown (Panther overrepresentation test, Bonferroni-corrected p<0.05). More detail is provided in Tables II and III in the online-only Data Supplement. (**C**) Effect of *JAG1* knockdown on selected inflammatory genes (Limma modified t test, Benjamini-Hochberg adjusted p-value). (**D**) Flow cytometric analysis of surface JAG1, VCAM1, DARC, and CX3CL1 in HUVECs treated with siRNA and stimulated as above. Graphs show fold change of mean fluorescence intensity relative to unstimulated cells from 5 independent experiments (means indicated by lines). Representative flow histograms are shown in Figure IE in the online-only Data Supplement. (**E**-**F**) RT-qPCR for VCAM1, HEY1, CX3CL1, and DARC using RNA isolated from HUVECs (**E**) exposed to IL-1β (5 ng/ml, 24 h) in the presence of a blocking antibody to JAG1 or isotype control, (**F**) plated on immobilized Jagged1 Fc (24 h). * p<0.05, ** p<0.01, *** p<0.001. Mann Whitney U (**D**-**E**) or Kruskall Wallis followed by Dunn´s multiple comparison test (**F**). See also Figure I in the online-only Data Supplement.

Figure 2: *JAG1 maintains the expression of genes supported by NOTCH1 in inflammatory activated endothelial cells, and its inhibition can be mirrored by targeting DLL4 or NOTCH1.* (**A**-**C**) Gene set enrichment analysis of IL-1β-stimulated HUVECs comparing cells treated with *JAG1* siRNA (siJAG1) to cells treated with scrambled siRNA (SCR), showing that *JAG1* knockdown mediated (**A**-**B**) negative enrichment of NOTCH1-supported genes (normalised enrichment score=-1,27, p<0.001, FDR=0.266, FWER=0.214) and (**A**, **C**) positive enrichment of NOTCH1-repressed genes (normalised enrichment score=1.47, p=0.091, FDR=0.096, FWER=0.044). (**D**-**F**) RT-qPCR for *VCAM1*, *HEY1*, *CX3CL1,* and *DARC* using RNA isolated from HUVECs (**D**) plated on immobilized DLL4-His (40 h). (**E**) exposed to IL-1β (5 ng/ml, 24 h) in the presence of a blocking antibody to DLL4 or isotype control, or (**F**) exposed to IL-1β (5 ng/ml, 24 h) in the presence of a blocking antibody to NOTCH1 or isotype control. * p<0.05, ** p<0.01, *** p<0.001, **** p<0.0001. Wilcoxon signed rank test (**D**) or Mann Whitney U (**E**-**F**). (**G**) Cell-based ELISA showing relative expression (OD) of VCAM1 after treatment with siRNA targeting *JAG1*, *DLL4,* or *NOTCH1* (27 nM, 72 h) and exposure to IL-1β (5 ng/ml, time indicated). Graphs show mean +/- SEM of values from at least 3 different donors. Inhibition of Notch components by siRNA reduced VCAM1 induction at the 2 hour (*DLL4*, p<0.0001), 3 hour (*NOTCH1*, p<0.01, and *DLL4*, p<0.0001), 4 and 6 hour (*JAG1*, p<0.001, *NOTCH1* and *DLL4*, p<0.0001), and 24 hour time points (*JAG1*, p<0.05, *NOTCH1*, p<0.001, *DLL4*, p<0.0001). Kruskall Wallis followed by Dunn´s multiple comparison test. See also Figure II in the online-only Data Supplement.

Figure 3: *Activation of endothelial NOTCH1 in inflamed human appendix.* (**A**) Immunostaining and (**B**) quantification of immunofluorescent csNICD1 signal in endothelial

cell nuclei (ERG positive) in biopsies from human appendix. (**A**) Mucosal vessel of inflamed human appendix. EC = endothelial cell, WBC = white blood cell, CEC = crypt epithelial cell. (**B**) Box plots show median +/- interquartile ranges, whiskers show the full range. **** p<0.0001 compared to biopsies scoring negative, Kruskall Wallis followed by Dunn´s multiple comparison test. (**C**-**H**) Representative images of tissue sections of non-inflamed (**C**, **D**, and **E**) and inflamed (**F**, **G**, and **H**) appendix, immunostained using antibodies targeting human csNICD1, VWF, and Hoechst nuclear stain. Details of antibodies and staining protocols are provided in Materials and Methods and in the online-only Major Resource Tables. Panels **C** and **F** show Hoechst signal in greyscale with VWF-signal in red. Panels **D** and **G** corresponds to panels **C** and **F**, respectively, and show the channel detecting csNICD1 signal in greyscale. Venules (v, red outlines), arterioles (a, blue outlines), and lymphatic vessels (L, yellow arrows) are indicated. Panels **E** and **H** show ~~merged~~ three-colour (csNICD1, VWF, and hoechst) higher magnification ~~3 channel~~ images of the areas identified by white boxes in panels **C** ~~**D**~~ and ~~**F**~~ **FG**, respectively. Scale bars represent 50µm. Note that crypt epithelial cells also show a positive signal for nuclear csNICD1. Exposures were identical for matched images **D** and **G**, and **E** and **H**, respectively. Image contrast was stretched to enhance visualization, applying identical settings for inflamed and non-inflamed tissues.

Figure 4: *Endothelial Notch signalling modulates inflammation in DNFB-induced contact hypersensitivity.* (**A**-**C**) Differences in ear thickness (∆µm) between DNFB-exposed and control ears shown for individual mice (circles) and as medians (bars). (**A**) Effect of systemic DAPT in wild-type C57BL/6J mice showing results of vehicle-treatment (light grey bars, n=12) and DAPT-treatment (white bars, n=12). (**B**) Effect of endothelial cell-specific knockout of Rbpj. Wild type (light grey bars, n=16) were compared to transgenic mice (white bars, n=14). (**C**) Effect of endothelial-specific overexpression of NICD1 (Nicd1iEC-OE). Wild type (white bars, n=15) were compared to Nicd1iEC-OE mice (light grey bars, n=16). (**D**) Automated quantification of CD45+ cells and (**E**-**F**) manual quantification of (**E**) intradermal CD3+ cells and (**F**) Ly6G+ cells in sections from DNFB-treated mouse ears, and (**G**) flow cytometry of collagenase-digested DNFB-treated ears showing CD11b+/Ly6C+ cells as a percentage of total CD45+ cells, all (**D**-**G**) comparing Nicd1iEC-OE mice to controls. (**A**-**G**) * p<0.05, ** p<0.01, *** p<0.001, **** p<0.0001, Mann Whitney U. (**H**) Endothelial cells isolated from collagenase-digested DNFB-treated ears from Nicd1iEC-OE (n=4) and WT mice (n=6) were submitted for transcriptional profiling. The heatmap shows common differentially expressed genes (adj.p<0.05, FC>1.3) in *NOTCH1* knockdown HUVECs stimulated with IL-1β (5 ng/ml, 4 h), in *JAG1* knockdown HUVECs stimulated with IL 1β (5 ng/ml, 24 h) (n=3), and in Nicd1iEC-OE mouse endothelial cells from DNFB-treated ears. (**I**) Automated quantification of VCAM1 signal in immunostained tissue sections from DNFB-treated ears of Nicd1iEC-OE and WT mice. Integrated Density values were normalized using the ratio between measured area in that section to the mean area of all sections measured. * p<0.05, Mann-Whitney U. See also Figure III in the online-only Data Supplement.

Figure 5 *NOTCH1-RBPJ binding premarks sites of RELA recruitment in endothelial cells and localizes in regions of inflammatory enhancers.* ChIP-seq for NOTCH1, RBPJ, and RELA was performed on HUVECs pooled from 13 different donors as described in ~~online-only~~

Materials and Methods. (**A**) Venn diagram showing peak overlap between sites occupied by NOTCH1 and RBPJ in unstimulated HUVECs and RELA in IL-1β-stimulated (5 ng/ml, 1 h) HUVECs. Numbers indicate total peak coverage for each transcription factor (in kilobases) and, for NOTCH1 and RBPJ, peak overlap with RELA in brackets. (**B**-**E**) Gene tracks of ChIP-seq signal for NOTCH1 and RBPJ near the transcriptional start sites of the (**B**) *HES1* and (**C**) *ICAM1* loci, and in inflammatory enhancer regions (defined by Brown et al, reference #17, indicated by red boxes along the x-axis, numbers refer to peak numbers in original publication) associated with the (**C**) *ICAM1*, (**D**) *VCAM1*, and (**E**) the *CCL2-CCL7-CCL11-CCL8* loci. The y-axis shows ChIP-seq signal (min-max signal given for each track type and location). The x-axis depicts genomic position. Called RBPJ and NOTCH1 peaks are shown as shaded regions and indicated by red arrows. Magnified tracks of regions marked by stipled boxes are shown in Figures 6A-B. See also Figures IV, V, and VI in the online-only Data Supplement.

Figure 6 *NOTCH1-RBPJ binding facilitates the activation of inflammatory enhancers.* ChIP-seq for NOTCH1, RBPJ, RELA, and H3K27ac was performed on HUVECs pooled from 13 different donors as described in ~~online-only~~ Materials and Methods. (**A**-**B**) Gene tracks of ChIP-seq signal for NOTCH1, RBPJ, RELA, and H3K27ac in inflammatory enhancer regions (defined by Brown et al, reference #17, indicated by red boxes along the x-axis, numbers refer to peak numbers in original publication) associated with the (**A**) *VCAM1*, and (**B**) *CCL2-CCL7-CCL11-CCL8* loci. The y-axis shows ChIP-seq signal (min-max signal given for each track type and location). The x-axis depicts genomic position. Called RBPJ peaks are shown as shaded regions and indicated by red arrows. (**C**) Venn diagram showing binding of RELA, RBPJ, and NOTCH1 in predefined inflammatory superenhancer regions. Numbers refer to the number of inflammatory enhancers with detected binding peaks for the indicated combination of transcription factors. (**D**) Mean peak intensity and (**E**) peak overlap (in kilobases) of H3K27ac signal in inflammatory enhancer regions in untreated (SCR med), IL-1β stimulated (SCR IL-1β), and NOTCH1-inhibited IL-1β stimulated (siN1 IL-1β) HUVECs. The significance of differences in mean peak intensities was measured using Wilcoxon signed rank test comparing SCR to SCR IL-1β ($p = 4.3 \times 10^{-8}$), siN1 IL-1β to SCR IL-1β ($p = 5.7 * 10^{-6}$), and siN1 IL-1β to SCR ($p = 0.0004$). See also Figures IV and V in the online-only Data Supplement.